FABRICATION OF VARIOUS METAL NANOSTRUCTURES
WITH
HOLE MASK COLLOIDAL LITHOGRAPHY

A THESIS SUBMITTED TO
THE GRADUATE SCHOOL OF NATURAL AND APPLIED SCIENCES
OF
MIDDLE EAST TECHNICAL UNIVERSITY

BY

İBRAHİM MURAT ÖZTÜRK

IN PARTIAL FULFILLMENT OF THE REQUIREMENTS
FOR
THE DEGREE OF MASTER OF SCIENCE
IN
PHYSICS

SEPTEMBER 2014

Approval of the thesis:

FABRICATION OF VARIOUS METAL NANOSTRUCTURES WITH HOLE MASK COLLOIDAL LITHOGRAPHY

submitted by **İBRAHİM MURAT ÖZTÜRK** in partial fulfillment of the requirements for the degree of **Master of Science in Physics Department, Middle East Technical University** by,

Prof. Dr. Canan Özgen
Dean, Graduate School of **Natural and Applied Sciences**

—————————

Prof. Dr. Mehmet T. Zeyrek
Head of Department, **Physics**

—————————

Assist. Prof. Dr. Alpan Bek
Supervisor, **Physics Department, METU**

—————————

Examining Committee Members:

Prof. Dr. Raşit Turan
Physics Department, METU

—————————

Assist. Prof. Dr. Alpan Bek
Physics Department, METU

—————————

Prof. Dr. Mehmet Parlak
Physics Department, METU

—————————

Assoc. Prof. Dr. H. Emrah Ünalan
Metallurgical and Materials Engineering Department, METU

—————————

Assoc. Prof. Dr. Mehmet Emre Taşgın
Institute of Nuclear Sciences, Hacettepe University

—————————

Date:

—————————

I hereby declare that all information in this document has been obtained and presented in accordance with academic rules and ethical conduct. I also declare that, as required by these rules and conduct, I have fully cited and referenced all material and results that are not original to this work.

Name, Last Name: İBRAHİM MURAT ÖZTÜRK

Signature   :

ABSTRACT

FABRICATION OF VARIOUS METAL NANOSTRUCTURES WITH HOLE
MASK COLLOIDAL LITHOGRAPHY

Öztürk, İbrahim Murat

M.S., Department of Physics

Supervisor   : Assist. Prof. Dr. Alpan Bek

September 2014, 75 pages

In this work, a novel surface nanostructuring technique called hole mask colloidal lithography (HMCL) is investigated and utilized to fabricate large area metal nanostructures with several geometries with photoresist over exposure and over develop as the undercutting method. Some extends of this method has been examined with constant angled deposition of dimer structures.

HMCL takes advantage of directional nature of thermal evaporation method for metal deposition through the nanoscale holes that are placed at a controlled distance away from the substrate surface. When an angle is applied between the normal vector of the surface and deposition direction, position of deposited material can be precisely controlled with respect to the hole. Colloidal nanospheres are employed to decorate the the surface with nanoscale holes, which offers fast and convenient large area decoration. What makes HMCL a superior lithography technique is its ability to parallelly fabricate both simple and complex nano geometries on large areas with variable min-

imum feature sizes and controllable surface coverages.

Hole generation is the most crucial part to achieve successful results with HMCL. It has been proposed and successfully employed in this thesis that undercutted holes at a controllable distance away from the surface can be fabricated by using a positive tone photoresist film on the surface as a sacrificial layer. Undercutting of photoresist is achieved by over exposure and over development. Spherical nanoparticles with two sizes (750 and 262 nm) are used to decorate over this resist film to later leave their places to holes.

Process steps are investigated and optimized for successful hole generation. Same procedure is found to be applicable to both sizes of holes. The success of the holes are investigated by deposition of dimers, trimers and quadromers on the substrates and examined with optical and electron microscopy.

After defining a successful procedure, positional precision examined by fabrication of close and distant dimer disks. Asymmetrical deposition possibilities with dimers are examined next. Three main asymmetrical structure fabrication possibilities are found. Asymmetrical thickness deposition, asymmetrical angled deposition and asymmetries arising from clogging of the holes. Several dimer structures are fabricated with asymmetrical thickness deposition and asymmetrical angle deposition under different conditions to comprehend the extend of asymmetrical possibilities.

Keywords: Metal nanoparticles, Nano fabrication, Plasmonics

ÖZ

DEŞİK MASKE KOLLOİDAL LİTOGRAFİSİ İLE ÇEŞİTLİ METAL NANOYAPILARIN ÜRETİLMESİ

Öztürk, İbrahim Murat

Yüksek Lisans, Fizik Bölümü

Tez Yöneticisi   : Yrd. Doç. Dr. Alpan Bek

Eylül 2014 , 75 sayfa

Bu çalışmada, orjinal bir yüzey nanoşekillendirme yöntemi olan deşik maske colloid litografisi (HMCL) incelenmiş ve büyük alanlarda çeşitli geometrilerde metal nanoyapılar üretmek için deşiklerin altını oyma methodu olarak fotoresist fazla pozlaması ve fazla geliştirilmesi ile kullanılmıştır. Bu yöntemin bazı sınırları ikili yapılarda sabit açılı kaplama ile incelenmiştir.

HMCL termal buharlaştırma yönteminin yönlenik kaplama özelliğinden yararlanır ve alttaş yüzeyinden kontrol edilebilir bir mesafede üretilen nano boyuttaki deşiklerden içeri metal kaplanması ile çalışır. Eğer yüzeyin normal vektörü ile kaplama yönü arasına bir açı verilirse, deşiklerden girerek kaplanan metalin kaplandığı yer hassaslıkla kontrol edilebilir. Deşiklerin üretimi için büyük alanları hızlı ve uygun bir şekilde küre parçacıklarla kaplayabilen kolloid litografisi kullanılır. HMCL'yi üstün bir yüzey şekillendirme yöntemi yapan şey paralel bir biçimde hem basit hem de karmaşık nano geometrilerin büyük alanlara, çeşitli minimum karakteristik boyutlarında

ve yüzey doluluklarında üretilebilmesidir.

Deşiklerin oluşturulması HMCL'nin başarılı olması için en önemli kısımdır. Yüzeyden kontrol edilebilir uzaklıklardaki altı oyulmuş deşiklerin oluşması için positif tonlu bir fotoresist filminin feda edilecek katman olarak kullanılabileceği tarafımızdan önerirlip başarı ile uygulanmıştır. Altı oyulmus deşikler fotoresistin fazla pozlanması ve fazla geliştirilmesi ile sağlanmıştır. İki farklı boyutta nanoküre (750 nm ve 262 nm) fotoresist yüzeyine dekore edilmiş ve daha sonra deşiklerin oluşturulmasında kullanılmıştır.

Deşik oluşturmasında kullanılan işlem basamakları incelenmiş ve optimize edilmiştir. Aynı basamakların kullanılan iki farklı boyutta da çalıştığı görülmüştür. Deşiklerin oluşum başarısı ikili, üçlü, ve dörtlü parçacıkların deşiklerden yüzeye kaplanması ile incelenmiştir. Oluşturulmuş yapılar optik ve elektron mikroskopları ile fotoraflanmıştır.

Başarı elde edilen işlem basamaklarına karar verilmesinden sonra, konum hassaslığı incelemeleri, çok yakın ve uzak ikililerin üretimi ile yapılmıştır. Asimetrik yapı üretim olasılıkları incelenmiş ve üç yöntemin bu konuda başarı sağlayabileceği bulunmuştur. Bunlar asimetrik kalınlıklı kaplama, asimetrik açı ile kaplama ve deşiklerin tıkanma etkisinden ortaya çıkan asimetirlerdir. Asimetrik ikililerden oluşan birkaç örnek asimetrik kalınlık kaplaması ve asimtrik açılı kaplama ile oluşturulmuş ve değişik parametreler altında incelenmiştir.

Anahtar Kelimeler: Metal nanoparçacıklar, Nano üretim, Plazmonik parçacıklar

To my family

ACKNOWLEDGMENTS

even a fraction of her efforts in any way. All I can do is to love her from deepest of my heart, as I do every single moment.

My parents Mustafa and Melek Öztürk deserves very special thanks, as they have been supportive in every step of my education. I also thank to my sisters Cansu and Göksu who gave me their pure love.

TABLE OF CONTENTS

LIST OF TABLES

TABLES

LIST OF FIGURES

FIGURES

xviii

LIST OF ABBREVIATIONS

CL Colloidal Lithography

IC   Integrated Circuit

PR   Photoresist

SP   Surface Plasmon

UV   Ultraviolet

DLW Direct Laser Writing

DUV Deep Ultraviolet

EBL Electrom Beam Lithography

EUV Extreme Ultraviolet

MNP Metal nano particle

SHG Second Harmonic Generation

SPL   Scanning Probe Microscopy

TPE   Two photon excitation

CARS Coherent anti-stokes Raman scattering

FIBL Focussed Ion Beam Lithography

HMCL Hole mask colloidal lithography

SERS Surface Enhanced Raman Scattering

CHAPTER 1

INTRODUCTION

The famous quote *"There is plenty of room at the bottom"* voiced by Richard Feynman more than half a century ago [1], has been confirmed by realization of countless possibilities bestowed to the science by the field of nanotechnology. Remarkable discoveries have been made and it is certain that there is still plenty of room in the nanoworld awaiting to be filled with curious researchers.

The study of plasmonics; a rapidly growing field of nanoscience; examines the phenomena arising from extraordinary optical response of metals at nanoscale. This response occurs by the resonator-like behavior of metallic nanostructures under electromagnetic excitation. Resonance modes of these structures called surface plasmon (SP) resonances and they occur by collective oscillations of free conduction band electrons. Surface plasmon resonances enables concentration and control of optical radiation in subwavelenth scale. In the case of surface plasmon resonances in nanoparticles, strong field enhancements in the vicinity of nanoparticles and enhanced far field scattering of distinct wavelengths are observed. Spectral position, shape and intensity of the resonance peaks are highly dependent to surrounding media, as well as structure geometry and size of the structure.

Far field scattering properties of plasmonic nanoparticles are used in sensing applications in several fields like biology and material science. High dependence of resonance wavelength to surrounding refractive index of a nanoparticle is used to detect trace amounts of molecules [2, 3, 4, 5]. Another widely known and examined application of SP resonance is surface enhanced Raman scattering (SERS) occurs by strong near field enhancements of nanoparticles. SERS have molecular level detec-

tion capabilities even a single molecule can be detected out of a solution with SERS [6, 7, 8, 9]. Several photovoltaic applications have been extensively investigated to increase the efficiency, by utilizing both scattering characteristics and enhanced near field strengths [10, 11, 12, 13].

With the development of lithography methods, more complex structures has been examined. Dimers are used to obtain so called *hot spots,* where the local field strength between the particles is many orders of magnitude higher than the exciting field at certain polarizations of incident radiation [14, 15]. Bow-tie structures enhance the local field strength orders of magnitude. Interactions of multiple plasmonic particles with close distances are examined, shifted resonance positions and new plasmonic resonance modes are observed due to interparticle interactions.[16, 17]. Enhanced nonlinear optical responses are observed arising from local field enhancement and coupled plasmon modes arising from interparticle interactions of nanoparticles [18, 19, 20].

Various theoretical approaches and models have been developed to explain SPs for simpler geometries. However; as the geometry gets complex, theoretical explanations become much more difficult to built from scratch. Most of the theoretical understanding develops with experiments. Experimental analysis methods play a very important role on understanding and developing a more comprehensive understanding about the subject.

This is where surface nanostructuring becomes momentous, both for understanding the surface plasmon phenomena and developing state of art devices exploiting its unique properties. Nanostructuring approaches for plasmonic applications are generally designed for either generation of a high resolution structures on small areas to conduct proof of principle experiments or fabrication of large area structures for industrial applications and like SERS substrates and photovoltaic (PV) applications. Proof of principle approaches generally uses lithographic methods that provide extended control over structure geometries like electron beam lithography (EBL) and scanning probe lithography (SPL), both of which offer high resolutions; however disallowing structuring of large areas. Large area structuring approaches mainly takes advantage of self assembly of nanostructures. Although, large area structuring is sup-

ported with self assembly methods, the drawback is the limited control over structure geometry.

A novel lithography method called Hole mask colloidal lithography (HMCL) can be utilized to fabricate large area controlled structures, for examination of collective responses of complex plasmonic nanostructure geometries. HMCL is a recently proposed method that can be viewed as a hybrid technique, as it allows large are structuring with extended control over structure geometry. In HMCL simple structures are distributed to surfaces by self assembly of colloidal particles. They later form various structure geometries that can be strictly controlled by angled directional deposition. In other words, exact positions of the structures are determined by self assembly of colloidal particles; while, structure geometry is highly controllable by the user. Large areas can be covered easily using colloidal lithography. Distribution of colloidal particles can even be made periodic. Minimum feature size of the generated structures is determined by the colloidal particle size which can vary from tens of nanometers to micrometers. One of the most important properties of HMCL is the possibility of nanoscale control over feature to feature distance. In other words; very small half-pitch distances of isolated particles can be fabricated with various geometries like dimers, trimers, tetramers etc. Moreover, complex geometries like asymmetrical multiple disks, chiral structures, split-rings, ecliptic disks, short rods, T shaped structures etc. can be fabricated with rotating angled deposition. This makes HMCL a perfect tool for examining plasmonic interactions of close plasmonic particles. Moreover, not only two dimensional but also three dimensional structures can be engineered with extended control over normal axis that HMCL offers within a single structure. This brings a significant freedom, that makes it possible to fabricate various asymmetries on the z-axis in a single structure [21].

Hole mask colloidal lithography is first proposed and applied by Fredriksson et al. in 2007 [22]. Several groups conducted experiments to comprehend the extend of HMCL. A motorized two-axis rotatable evaporation holder used to gain three dimensional control over the structures by Zhao et al., which highly increased the number of possible geometries [23, 24, 21].

This thesis is written on the basis of the experiments conducted for utilization of

HMCL. Chapter 2 is designed to give the reader a brief background information about the surface plasmons. For this purpose after a brief review of the historical development and simple yet efficient theoretical approaches are investigated. Several applications and their backgrounds are discussed. In Chapter 3 some common surface nanostructuring methods are discussed under two main sections; controlled approaches and self assembly of nanostructures. Advantages and disadvantages of each method over each other are discussed. Detailed information about HMCL is given in Chapter 4 including conducted experiments and possible improvements. Detailed procedures, successful and unsuccessful experiments are also discussed throughout the chapter. Conclussions and future improvements are discussed in Chapter 5.

CHAPTER 2

SURFACE PLASMONS

Plasmonic interactions arise from collective electron oscillations of metal's electron cloud induced by electric field of an exciting light. Resonances arise from these oscillations can be referred as surface plasmons (SP). Probably the most remarkable property of SP is its ability to confine optical energy into nanoscale, that is much smaller than the diffraction limit. Surface plasmons come into existence only at the interfaces of materials having oppositely signed dielectric constants (eg. metal-dielectric interface) via coupling of photons into plasmons. There are two fundamental plasmonic excitations, surface plasmon polaritons (SPPs) and localized surface plasmons (LSPs). Former propagates on planar metal-dielectric interfaces, while the latter is an oscillation on closed surface of a nanostructure. SPP's will be introduced in but not be discussed to details in upcoming sections as the LSP, which is the main interest of this thesis.

2.1 A Brief History

The first known application of surface plasmons in the history of humankind is a piece of art known as *Lucurgus Cup*, most probably accidentally manufactured in the fifth century and become famous because of its unique response to light. What attracted people's attention to this piece was the color difference of reflected and transmitted light, see Fig.2.1. Today one can still see some church windows that unknowingly use the surface plasmons. The scientific explanation of how such phenomena occurred surfaced much later than its practice.

5

Figure 2.1: Famous Lycurgus cup. Left: Front illuminated , Right: Back illuminated

First controlled experiments on the subject is conducted in 19th century by Michael Faraday (1781-1867), he synthesized colloidal solutions composed of gold nanoparticles, examined them and called it *Activated Gold* [25]. About 40 years later than Faraday's work on synthesis of colloidal gold particles; Richard Zsigmondy managed to observe colloidal gold particles with the ultra-microscope that he invented [26]. This followed by the theoretical calculations made by Gustav Mie (1869-1957) [27] by solving Maxwell's equations for absorption and scattering properties of spherical metal nanostructures. The calculations made by Mie are still used widely by plasmonics society [28, 29]. Robert Wood discovered another interesting plasmonic phenomenon in 1902 [30]. When studying reflections from metallic gratings he found spectral features he could not explain. Later they turned out to be surface plasmon resonances excited in the gratings [31].

The term *plasmon* is used by David Pines for the first time to describe high frequency electron oscillations that occurs in metals in the 1950s [32]. Plasmon is a quasiparticle resulting from quantization of plasma oscillations. in the mid 1970s, Martin Fleischman ans Richard van Duyne and coworkers observed intense Raman scattering signals from molecules on rough metal surfaces and called it *surface enhanced Raman scattering* (SERS). It was recognized that SERS is due to strongly enhanced local electromagnetic fields generated by surface plasmon resonances.

Until the end of 20th century researches on subjects occupying surface plasmons handled independently, one of the turning points leading a unified understanding was the observation of *extraordinary optical transmission* (EOT). EOT is transmission of light from sub-wavelength apertures on thick metal films several orders of magnitude

higher than the predicted values [33, 34]. This effect explained by plasmon resonances that occurs in the apertures. Possibility of confinement and control of light in sub-nanometer scale highly increased the popularity of plasmonic interactions and the field of *plasmonics* was born and shaped as it is today.

2.2 Theoretical Considerations and Applications

2.2.1 SPPs and LSPs

As previously mentioned surface plasmon subject includes two main interactions SPPs and LSPs. SPPs are surface electromagnetic waves that guided through the surface of metals at the metal-dielectric interfaces. They can propagate on the surface for tens to hundreds of micrometers and fades away because of absorption in the metal and scattering through the dielectric medium (Figure 2.2 a). A comprehensive information on SPP's can be found in Maier chapter 2 and 3 [35].
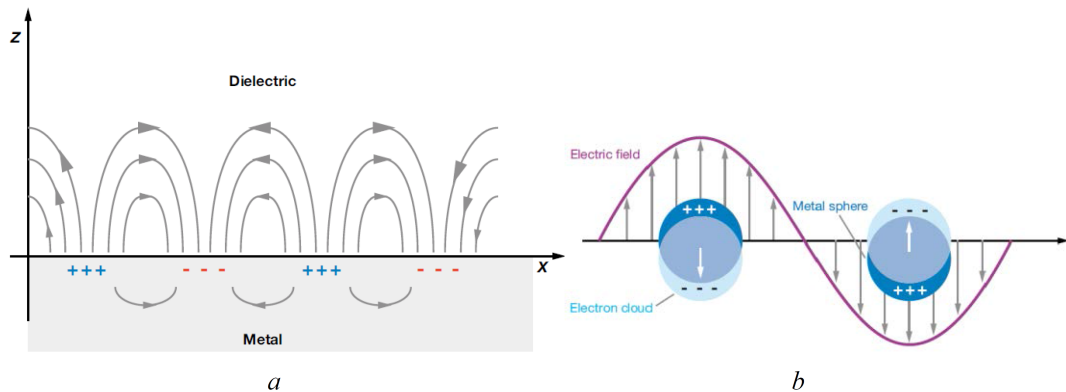
Figure 2.2: Left: Surface plasmon polaritons generated on a metal dielectric surface. (b) Excitation of a localized surface plasmon resonance in a metal nanoparticle by an incident radiation

Plasmonic interaction of sub-wavelength metal nanoparticles with light called LSPs. When a metal nanoparticle with much smaller size than electromagnetic wavelength is under an external oscillating field, it experiences its effects on its electron subsystem [36] (Figure 2.2 b). A metal nanoparticle can be seen as a resonator of electrons with moderate damping. Closed surface of the metal nanoparticle exerts restoring forces to the electrons driven by the field. This arises resonance modes. The resonant oscillation amplitude can by far surpass excitation amplitude, this cor-

responds to strong local enhancement of electromagnetic field in the vicinity of the particle [37, 38, 28].

2.2.2 Polarizability of a Nanoparticle: Quasi-static Approximation

When the particle diameter is much smaller than the wavelength of exciting light *quasi-static approximation* can be used to simplify field distribution problem to a metal particle under constant field. Time dependence term arising from oscillating field can be applied to the solution later. For simplicity, consider a spherical metal nanoparticle of radius a inside a dielectric medium. Let, $\vec{E} = E_0 \hat{z}$, the dielectric function of the surrounding medium be ε_m and the dielectric function of sphere be $\varepsilon(\omega)$.

Solution of the Laplace's equation for spherical conductor under constant electric field can be used to calculate the field inside and outside of the sphere. Electric potential inside and outside of the sphere can be written as:

$$\Phi_{in}(r, \theta) = \sum_{l=0}^{\infty} A_l r^l P_l(cos\theta) \tag{2.1a}$$

$$\Phi_{out}(r, \theta) = \sum_{l=0}^{\infty} \left[B_l r^l + C_l r^{-(l+1)} \right] P_l(cos\theta) \tag{2.1b}$$

Where $P_l(cos\theta)$ is the Legendre polynomials of order l and θ is the angle between position vector and the z-axis.

The boundary conditions at $r \to \infty$; $\Phi_{out} \to -E_0 z = E_0 r cos\theta$. This implies that $B_1 = -E_0$ and $B_l = 0$ for $l \neq 1$.

A_l and C_l can be found from the boundary conditions at the interface $(r = a)$, corresponding boundary conditions are:

$$-\frac{1}{a}\frac{\partial \Phi_{in}}{\partial \theta}\bigg|_{r=a} = -\varepsilon_0 \varepsilon_m \frac{\partial \Phi_{out}}{\partial \theta}\bigg|_{r=a} \tag{2.2a}$$

for equality of tangential components of electric field and;

$$-\varepsilon_0 \varepsilon(\omega)\frac{\partial \Phi_{in}}{\partial r}\bigg|_{r=a} = -\varepsilon_0 \varepsilon_m \frac{\partial \Phi_{out}}{\partial r}\bigg|_{r=a} \tag{2.2b}$$

for normal components of electric displacement.

Application of these boundary conditions leads to $A_l = C_l = 0$ for $l \neq 1$. The potentials evaluates as:

$$\Phi_{in} = -\frac{3\varepsilon_m}{\varepsilon(\omega) + 2\varepsilon_m} E_0 r cos\theta \qquad (2.3a)$$

$$\Phi_{out} = -E_0 r cos\theta + \frac{\varepsilon(\omega) - \varepsilon_m}{\varepsilon(\omega) + 2\varepsilon_m} E_0 a^3 \frac{cos\theta}{r^2} \qquad (2.3b)$$

Equation 2.3b describes a superposition of the applied field and a dipole at particle center. When a dipole moment term $(\vec{p})$ introduced, the equation 2.3b becomes;

$$\Phi_{out} = -E_0 r cos\theta + \frac{\vec{p}.\vec{r}}{4\pi\varepsilon_0\varepsilon_m r^3} \qquad (2.4)$$

where

$$\vec{p} = \vec{E_0} 4\pi\varepsilon_0\varepsilon_m a^3 \frac{\varepsilon(\omega) - \varepsilon_m}{\varepsilon(\omega) + 2\varepsilon_m} \qquad (2.5)$$

The polarizability (α), is introduced as $\vec{p} = \varepsilon_0\varepsilon_m\alpha\vec{E_0}$, and found as;

$$\alpha = a^3 \frac{\varepsilon_m(\varepsilon(\omega) - \varepsilon_m)}{\varepsilon(\omega) + 2\varepsilon_m} \qquad (2.6)$$

It is clear from equation 2.6 that polarizability experiences a resonant enhancement at;

$$Re[\varepsilon(\omega)] = -2\varepsilon_m \qquad (2.7)$$

This result is very important in understanding optical phenomena arising from metallic nanoparticles. The frequency of this resonance falls into the visible spectrum only for gold and silver [35]. To understand the resonance phenomena better; an introduction about optical properties of metals will be given in the next subsection before going further into resonance properties of plasmonic structures.

2.2.3 Dielectric Function of Metals

Optical properties of metals can be explained by a *electron plasma model* over a limited frequency range. This approach is also called *Drude model* for optical properties of metals. In plasma model a free electron gas is driven by an external electric field.

9

Although the model is not completely realistic for noble metals at optical frequencies, it is a good place to build our understanding about optical properties of metals.

Motion of electrons (with effective mass m) is damped by collisions that occurs with characteristic collusion frequency γ. Equation of motion for an electron of plasma that is driven by an external electric field $\vec{E}(t)$, can be written as;

$$m\ddot{\vec{x}} + m\gamma\dot{\vec{x}} = -e\vec{E}(t) \tag{2.8}$$

Taking into account $\vec{E}(t) = \vec{E}_0 e^{-i\omega t}$ yields;

$$\vec{x}(t) = \frac{e}{m(\omega^2 + i\gamma\omega)}\vec{E}(t) \tag{2.9}$$

Total macroscopic polarization of the electron gas can be found by multiplying each electrons contribution with number density of electron gas and electron charge

$$\vec{P}(t) = -\frac{ne^2}{m(\omega^2 + i\gamma\omega)}\vec{E}(t) \tag{2.10}$$

Electron cloud can be considered as a linear isotropic media, where $\vec{P} = \varepsilon_0\chi\vec{E}$, where $\chi = \varepsilon - 1$ [39],

$$\varepsilon_0(\varepsilon(\omega) - 1) = -\frac{ne^2}{m(\omega^2 + i\gamma\omega)} \tag{2.11}$$

By substituting *plasma frequency* $\omega_p^2 = \frac{ne^2}{\varepsilon_0 m}$ into equation 2.11, we get complex dielectric function of the electron plasma as

$$\varepsilon(\omega) = 1 - \frac{\omega_p^2}{\omega^2 + i\gamma\omega} \tag{2.12}$$

We can separate this into imaginary and real parts of equation 2.12 as;

$$Re[\varepsilon(\omega)] = 1 - \frac{\omega_p^2\tau^2}{1 + \omega^2\tau^2} \tag{2.13a}$$

$$Im[\varepsilon(\omega)] = \frac{\omega_p^2\tau}{\omega(1 + \omega^2\tau^2)} \tag{2.13b}$$

τ is relaxation time of electron gas, which is inverse of characteristic collision frequency; $\gamma = \frac{1}{\tau}$ [40].

When $\omega > \omega_p$ the response of metals is called transparency regime. The electron plasma cannot support frequencies higher than the plasma frequency. When the exciting frequency is higher than the plasma frequency, metals does not retain their

metallic character. They simply transmit incoming radiation. It is wise to consider just $\omega \leqq \omega_p$ region when examining equations 2.13a and 2.13b.

The dielectric function found in equation 2.12 by Drude model for optical properties of metals is valid at low ω values. The imaginary component of the dielectric function increases when photon energies are above the threshold of transitions between electronic bands. Transitions induced by these photons are called interband transitions. For some metals like gold and copper, interband transitions occur at the visible frequencies, this causes absorption of some frequencies, which gives them their specific color. Interband transition effects are clearly visible in Figure 2.3 and 2.4 for Au and Ag respectively [35]. As seen in the graphs interband transitions are more effective for Au in the visible range, making Drude model inadequate. For Ag however; the model seems to be valid in the visible range.
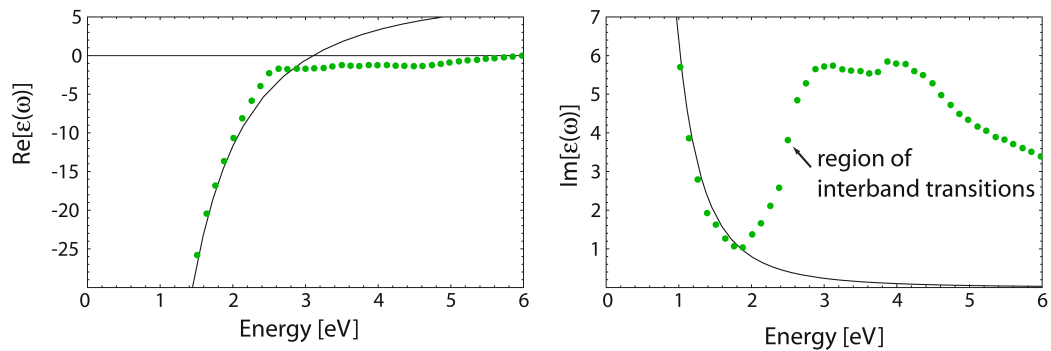
Figure 2.3: Dielectric function of metals by Drude model (solid line) fitted to experimental values for the dielectric fuction of gold (green dots) [41]. Interband transitions limit the validity of this model and higher frequencies. Adopted from [35]
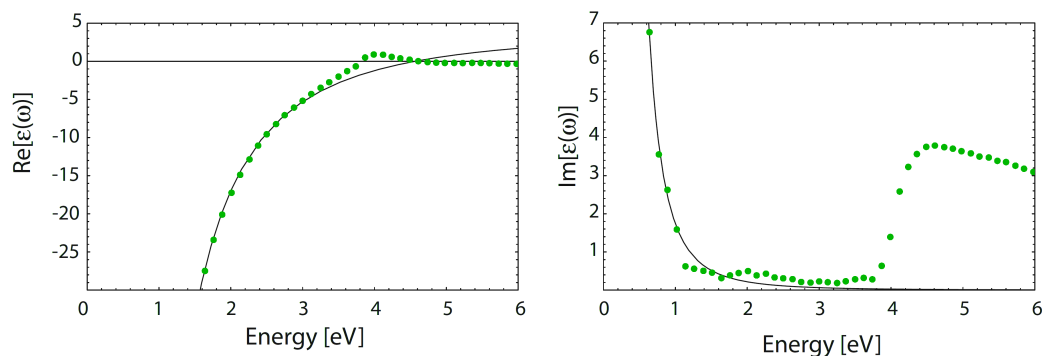
Figure 2.4: Dielectric function of metals by Drude model (solid line) fitted to experimental values for the dielectric fuction of silver (green dots) [41]. Adopted from [35]

2.2.4 Absorption and Scattering

The polarizability found in equation 2.6, experiences a resonant enhancement at;

$$Re[\varepsilon(\omega)] = -2\varepsilon_m \tag{2.14}$$

The spectral position of the resonance is very sensitive to small changes of surrounding medium especially for gold nanoparticles (figure 2.3). According to the Drude model the resonance frequency red-shifts as the dielectric constant of surrounding media increases.

Electric fields inside and outside of the particle can be evaluated by applying $\vec{E} = -\nabla\Phi$ to equation 2.3b and 2.3a. It results;

$$\vec{E}_{in} = E_0 \frac{3\varepsilon_m}{\varepsilon(\omega) + 2\varepsilon_m}(cos\theta\hat{r} + sin\theta\hat{\theta}) \tag{2.15a}$$

$$\vec{E}_{out} = E_0(cos\theta\hat{r} + sin\theta\hat{\theta}) + \frac{(\varepsilon(\omega) - \varepsilon_m)a^3}{\varepsilon(\omega) + 2\varepsilon_m}\frac{1}{r^3}E_0(cos\theta\hat{r} + sin\theta\hat{\theta}) \tag{2.15b}$$

Near the surface of the nanoparticle where $a \sim r$ equation 2.15b simplifies to:

$$\vec{E}_{surface} \simeq E_0(cos\theta\hat{r} + sin\theta\hat{\theta}) + \frac{(\varepsilon(\omega) - \varepsilon_m)}{\varepsilon(\omega) + 2\varepsilon_m}E_0(cos\theta\hat{r} + sin\theta\hat{\theta}) \tag{2.16}$$

At resonance where $Re[\varepsilon(\omega)] = -2\varepsilon_m$ a very strong near field enhancement is expected. Near field strength $|\vec{E}_{nf}|^2$ drops as distance from the particle increases. Up to order of 10^5 field enhancements are possible [42].

Scattering and absorption coefficients of a small particle can be calculated as:

$$C_{scat} = \frac{k^4}{6\pi}|\alpha|^2 = \frac{8\pi}{3}k^4a^6\left|\frac{\varepsilon(\omega) - \varepsilon_m}{\varepsilon(\omega) + 2\varepsilon_m}\right|^2 \tag{2.17a}$$

$$C_{abs} = kIm[\alpha] = 4\pi ka^3\left[\frac{\varepsilon(\omega) - \varepsilon_m}{\varepsilon(\omega) + 2\varepsilon_m}\right] \tag{2.17b}$$

From scattering and absorption coefficients, it must be noted that at resonance frequency both scattering and absorption is enhanced. Remark should be made here to the size dependencies, absorption is dominated for small particles while as particles size gets bigger scattering becomes the more dominant effect, thus increasing the scattering portion of incident energy (Figure 2.5)
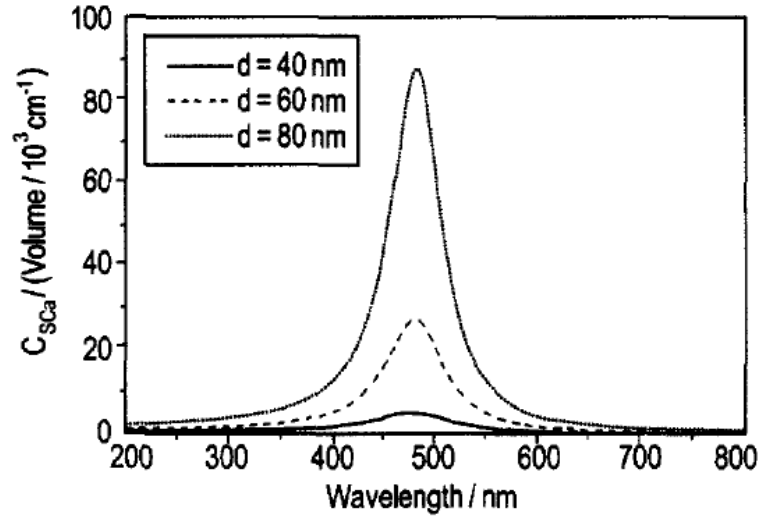
Figure 2.5: Scattering crosssections of silver nanoparticles with different particle diameters

One should note all off these results are found with imperfect theories, based on many approximations and only viable when many conditions are matched. However they perfectly explain the plasmonic resonance phenomena in easier terms.

It should also be noted that the polarizability's resonance condition is highly dependent on particle shape as seen in the figure 2.6, Observed resonance positions highly dependent to the shapes of nanoparticles.
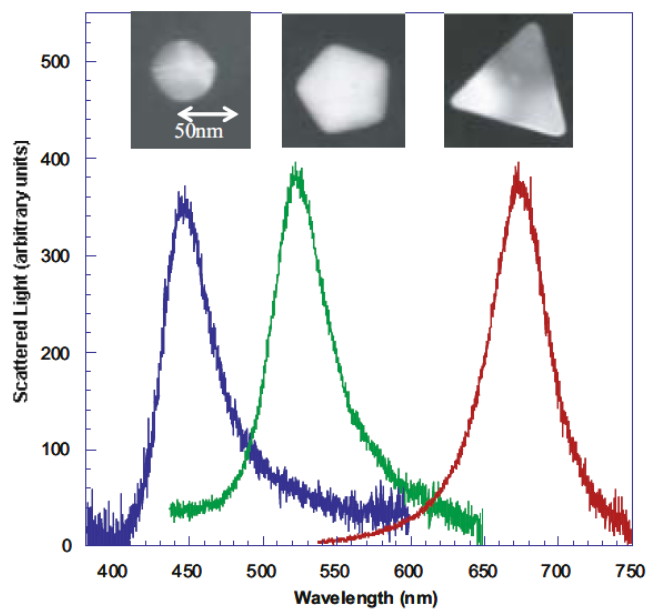
Figure 2.6: Plasmonic resonance of particles with diffrent geometries. Adopted from [36]

13

2.2.5 Coupling of Close Plasmonic Nanoparticles

Individual plasmonic oscillations in close plasmonic particles can couple via their near field interactions, this results coupled plasmonic resonance modes. In a simpler case; when two metal nanoparticle are in proximity with each other, near fields of these particles can interact with each other. The electric field felt by each particle is the superposition of incident field and the near field of the other particle.

$$\vec{E} = \vec{E}_0 + \vec{E}_{near} \tag{2.18}$$

This interaction results coupled plasmon resonance modes and the resonance position shifts to lower frequencies [43]. Storhoff et al. examined the red shift of resonance wavelength on an assembly of closely packed gold nanoparticles. Increasing number of particles in the assembly and decreasing interparticle distance are found to increase total amount of the red shift when compared to isolated particle resonance position [44].

A more intuitive investigation on plasmon coupling has been made with metal nanodisk dimers fabricated with electron beam lithography (EBL) with different interparticle distances. It has been found that plasmon coupling is polarization dependent. Figure 2.7 shows total red shift of extinction spectrum of nanodisk dimers with different gaps between the disks when illuminated by polarization parallel and perpendicular to interparticle axis. It is clearly observed that redshift of resonance wavelength occurs when the incident light is parallelly polarized to the interparticle axis indicating formation of plasmon coupled resonance modes, as expected the shift is increased as interparticle distance is decreased. On the other hand almost no shift observed for polarization perpendicular to the interparticle axis [28, 43, 45].
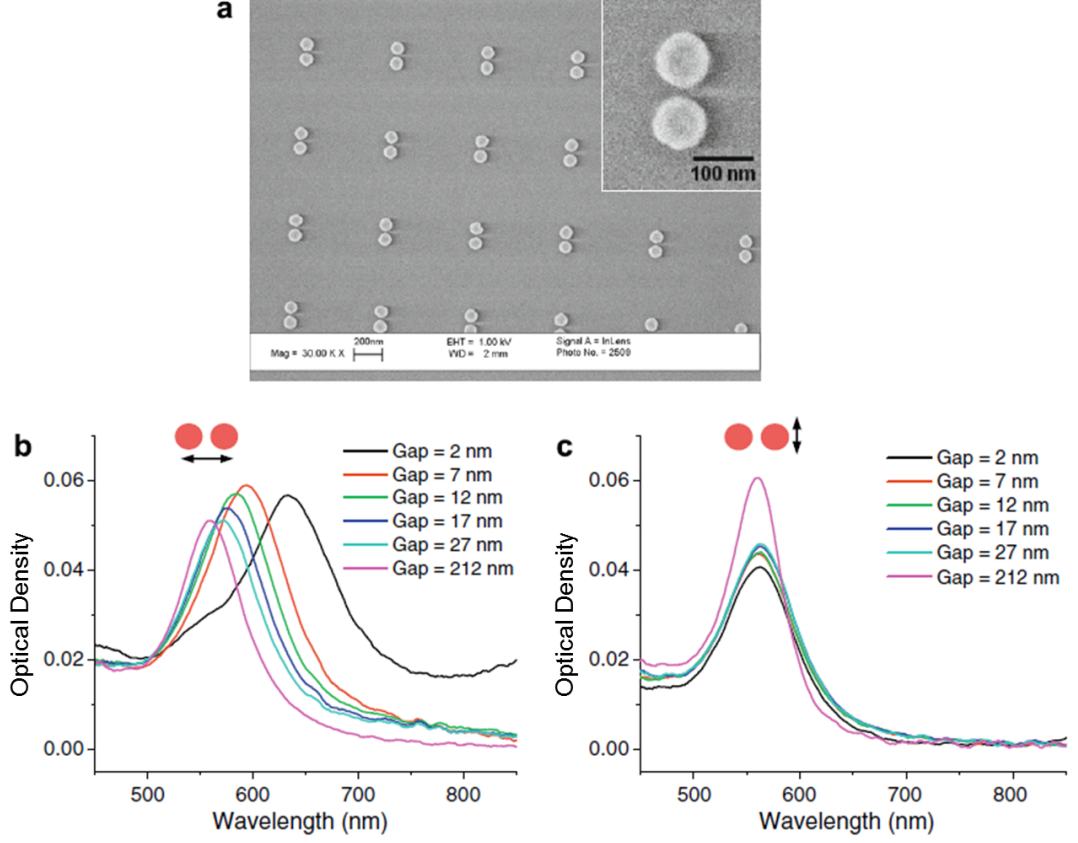
Figure 2.7: (a) SEM image of EBL fabricated 88 nm diameter gold nanodisc dimers. 12 nm interparticle separation. (b) and (c) show experimentally found extinction spectra of the array of dimers that is obtained by microabsorption spectroscopy for polarization along the interparticle axis and polarization orthogonal to the inter-particle axis respectively. Compared interparticle gaps are 2, 7, 12, 17, 27, and 212 nm. Adopted from [45].

2.2.6 Plasmon Enhanced Optical Nonlinearities

Strong localized electromagnetic near field resulting from plasmonic resonances may enhance nonlinear optical effects of surrounding medium in the vicinity of metal nano structures. The probability of nonlinear optical effects in a medium depends on the field strength superlinearly. The response of a material to electromagnetic field is described by the polarization of the material as:

$$P = \varepsilon_0 \left[\chi^{(1)} E + \chi^{(2)} E^2 + \chi^{(3)} E^3 + ... \right] \tag{2.19}$$

where $\chi^{(n)}$ is the nth-order susceptibility of the material. Higher order terms corre-

15

sponds to respective nonlinear optical processes. Figure 2.8 shows some fundamental nonlinear optical processes; Two photon excitation (TPE) and second harmonic generation (SGH) are second order nonlinear processes while coherent anti-Stokes Raman scattering (CARS) resulting from degenerate four wave mixing is a third order nonlinear process.

At low field intensities higher order terms may be omitted, however at high intensities they may reach considerable levels [39]. Strong near field enhancements may greatly enhance nonlinear effects as they are superlinearly dependent to the field intensity.
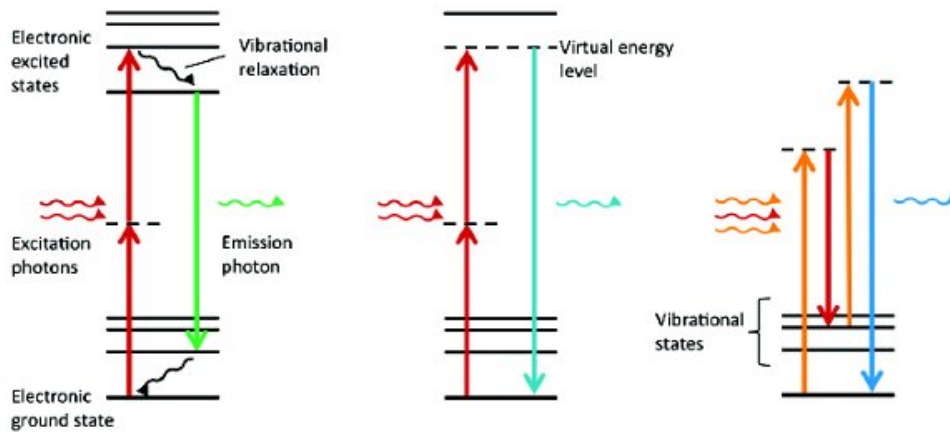
Figure 2.8: (Left) Two photon excitation, where two photon is absorbed by the material and flurescence signal is emitted. (Middle) Second harmonic Genaration, where two photons are absorbed and a photon with half wavelength is emitted. (Right) coherent anti-stokes Raman scattering (CARS), where two photons stimulate selected vibrational mode. Adopted from [46].

Symmetry of material is a constraint for nonlinear optical effects. While third order effects are supported by any geometry, it is very cumbersome to observe second order effects with centrosymmetric materials [28, 47].

Recent theoretical work by Turkpence et al. shown that nonlinear processes can be controlled by interaction with a molecule or quantum dot sandwiched between two metal nanoparticles (MNPs). Strong local electromagnetic field between the particles (Figure 2.9).
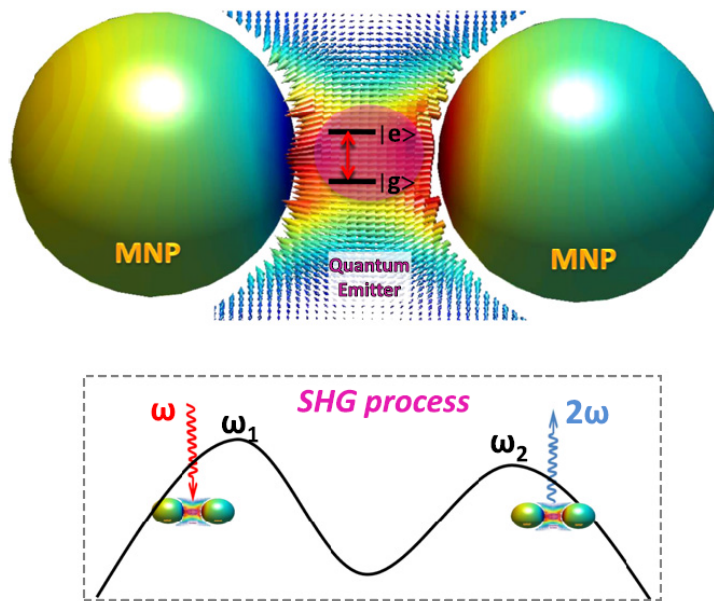
Figure 2.9: Top: Two metal nanoparticles and a quantum emitter ,with level spacing of two incident energy, between them. Bottom: Second harmonic response induced by incident frequency at coupled plasmon resonance mode of the dimer. Reprinted with permission from [20].

CHAPTER 3

SURFACE NANOSTRUCTURING

Fast emerge of nanotechnology has led development of many surface patterning techniques for the fabrication of micro and nano scale altered devices. This section will give an overview over common techniques, as well as their advantages and disadvantages over each other. Surface nanostructuring approaches can be divided into 2 parts as controlled approaches and self assembly of structures. Former, has some level of control over generated structures while latter depends on self assembly of structures in a system that is given some directions with initial conditions.

3.1 Controlled Approaches

Controlled structuring techniques are widely used as they allow some level of control over every structure to be generated. There is generally a trade off between speed and level of control, which ultimately limits area compatibility of nanometer scale fabrication.

Resist films are generally the workhorse of most controlled and even uncontrolled lithographic methods. Resists in lithography is a sensitive material to radiation that changes its solvability in certain developers when exposed with that radiation, this radiation can be light as well as electron or another particles. Commercial resists are named with the type of irradiation that they are sensitive to i.e. photoresist (PR) or electron beam resist. Either negative tone or positive tone photoresists can be used. If a positive tone photoresist used, exposed places decomposes in developer and it is vice versa for negative tone photoresist. Both positive and negative resists can be

found commercially with different properties. There are also some photoresists that can be used either as negative or positive when applied with different recipes (eg. AZ-5214 image rehearsal photoresist).

3.1.1 Direct Laser Writing (DLW)

A modulated laser beam scans the surface of a photosensitive material with desired fashion using reflected laser beam from galvanometric scanners. However, some amount of total radiation energy is required to alter properties of the photosensitive film, generally ultra-fast pulsed lasers are used to meet these requirements in short exposure times. This increases the cost of the system. Wavelength of the laser is the main limit on the minimum feature size. Generally near infrared lasers are used because of their availability which limits the feature sizes to micrometer range. To sum up DLW is fast and convenient for generating various structures with micrometer features. Lasers with far UV outputs (several hundreds of nm wavelengths) has been utilized for better resolution with DLW [48].

A more advanced version of DLW is called multiphoton lithography, With multiphoton lithography 3-D patterns can be generated by usage of a nonlinear optical process called two photon absorption. The used photoresist in multiphoton lithography is not sensitive to laser wavelength; but, its second harmonic (half of its wavelength). Since second order optical nonlinear processes are very rare at low intensities and probability of SGH proportional to square of the incident intensity ; in the close vicinity of focal point of laser beam, SGH probability highly increases exposing photoresist in the close vicinity of focus of the beam. When a negative tone photoresist is used, after development only the areas exposed with the close vicinity of the focal point of the beam stays on the surface while rest of the PR dissolves. An example structure fabricated with multiphoton lithography is given in figure 3.1 [49].

3.1.2 Electron Beam Lithography

Similar to DLW, electron beam lithography (EBL) consists of controlled maskless exposure of a resist surface. Instead of light, electrons are used and magnetic condenser
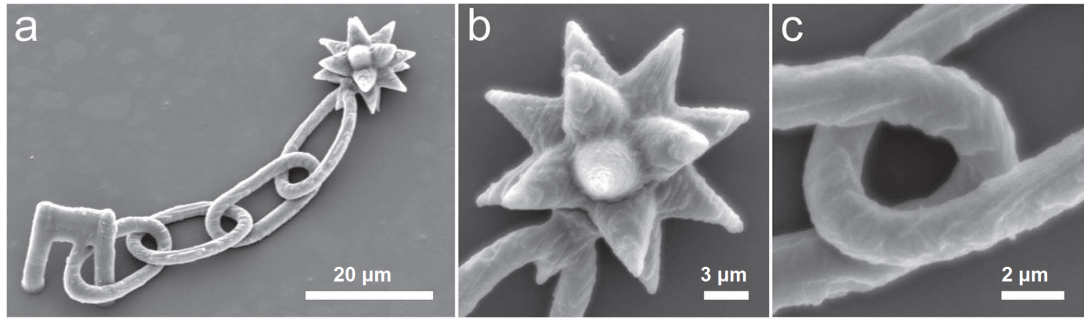
Figure 3.1: 18 point spiked star and 4 chain links micro-structure fabricated with multiphoton lithography. Adopted from [49].

lenses are used to control scanning beam. As in any photolithography, exposed or unexposed parts dissolves in the developer. EBL is used to generate high resolution structures on the surfaces and minimum features are within sub-ten nanometer range. Since the size of the beam at the focal point may reach sub-nanometer range, minimum feature size achievable is mostly governed by the exposure characteristics of the resist film. Most frequently used resist for electron beam is poly(methyl methacrylate) (PMMA), though some photoresists, like SU-8 negative tone and AZ-5214 image rehearsal, are both sensitive to UV and e-beam radiation. Minimum feature sizes as small as 4 nm and half pitch size (half periodicity of repeating structures) can be ~5 nm [50, 51, 52]. E-beam writing is extremely slow because of high dosage needs of resist films and dot by dot serial fashion writing of structures. Writing speed can be up to ~20 minutes for even 100x100 micrometer square areas. Slow throughput decreases large area reliability.

3.1.3 Scanning Probe Lithography

Scanning probe lithography (SPL) is an application of scanning probe microscopes (SPM). SPL works by fine moving a very sharp tip on the surface to change surface properties of the substrate by heating, scratching, oxidizing, exposing or transferring of particles [54]. Although; each have a specific applications, the last one is more commonly used. Transferring of particles with an scanning probe system, also called dip-pen lithography; works by grabbing one or more particles that are distributed on the surface and placing them to desired places. Best resolution (molecular level)
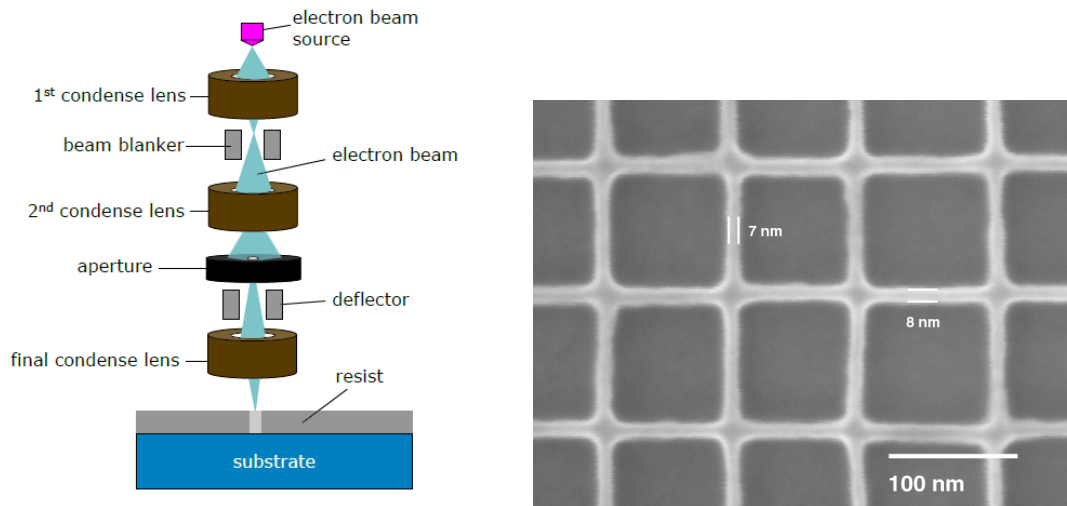
Figure 3.2: Left: Schematic illustration of an electron beam lithography setup; Right: A state of the art EBL generated pattern (retrieved from [53]).

among all other lithography methods is achieved by dip-pen lithography [55]. Although the resolution is very high, throughput is incredibly low with SPL. Large area structuring with many features would be impossible using any of the SPL methods. SPL methods widely used for *proof of principle* experiments on very small areas [14].
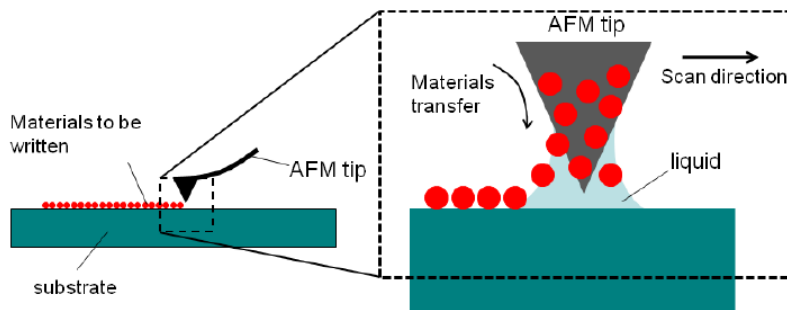
Figure 3.3: Schematic illustration of dip pen lithography (retrieved from [56]).

3.1.4 Photolithography

In photolithography, surface is structured with the features of a pre-fabricated photomask. A photosensitive film is exposed through the features on the photomask with UV radiation. The features are transferred to underlying resist after the development. Many samples can be structured fast and conveniently with the same features as the
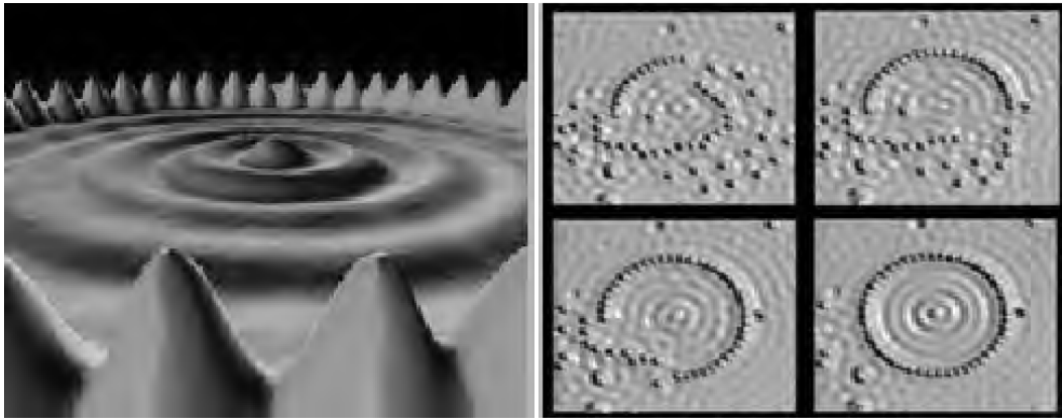
Figure 3.4: Atom by atom manipulation of xenon atoms on cooper surface to generate an artificial ring of 7 nm diameter with scanning tunneling microscope. The artifical ring is called quantum corral which confines the electrons on a metal surface [57].

used photomask, that made the photolithography a workhorse for commercial IC fabrication. Photomasks are still fabricated by other controlled methods (usually DWL or EBL) but after fabrication of photomask, they can be reproduced very easily. Main limitation of photolithography is feature size that is limited by the diffraction limit of used illumination source. Standart UV photolithography uses visible g-line (436 nm) and UV i-line (365 nm) that cannot handle sub-micrometer features. This limitation led the evaluation of illumination lamps and optics through lower wavelengths. Deep UV lamps and lasers are developed and used for smaller features (~500 nm). Extreme UV sources (~13.5 nm wavelength) and even X-ray sources (~0.5 nm wavelength) developed for high resolution photolithography . Photolithography with X-rays can support features that is smaller than EBL supports. [58, 59].
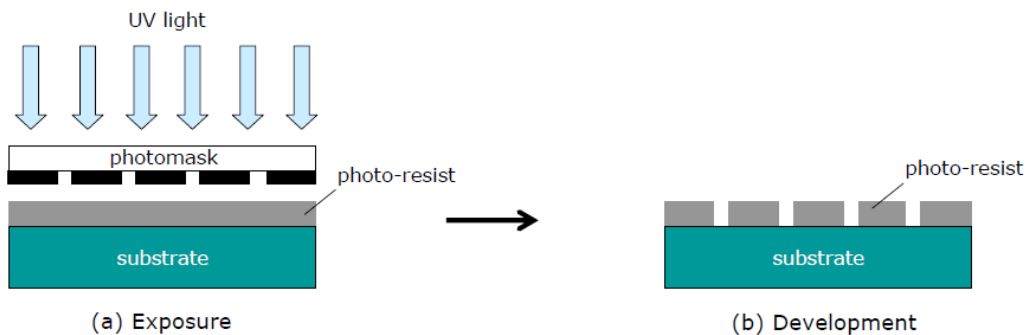
Figure 3.5: Illustration of a typical photolithography process.

23

3.1.5 Nanoimprint Lithography

Nanoimprint lithography (also known as soft lithography) is used to transfer fabricated structures on desired surfaces like photolithography. Nanoimprint lithography works the same way as an old typewriter, where pre-fabricated letter stamps transfer letters to paper with ink. In nanoimprint lithography, transferring can be done by several ways like transferring of molecules (Figure 3.6) or stamping a heated polymer and cooling. It promises high throughput, high resolution with relatively lower cost, compared to photolithography. Moreover limitations of photolithography caused by diffraction limit of light is not an issue for nanoimprint lithography [60, 56].
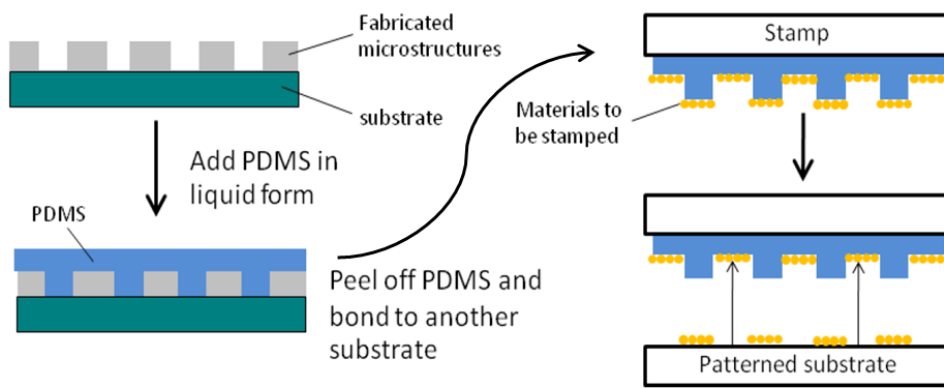
Figure 3.6: Schematic illustration of nanoimprint lithography by transfer of molecules.

3.1.6 Interference Lithography

Interference pattern of multiple coherent light beams can be used to expose photoresist to generate periodic structures on the surfaces. To generate patters a coherent laser beam is divided into multiple beams and beams are expanded to cover the surface. Beams traveled different distances, meets again at the surface and generate an interference pattern because of the phase difference between the beams (fig 3.7).
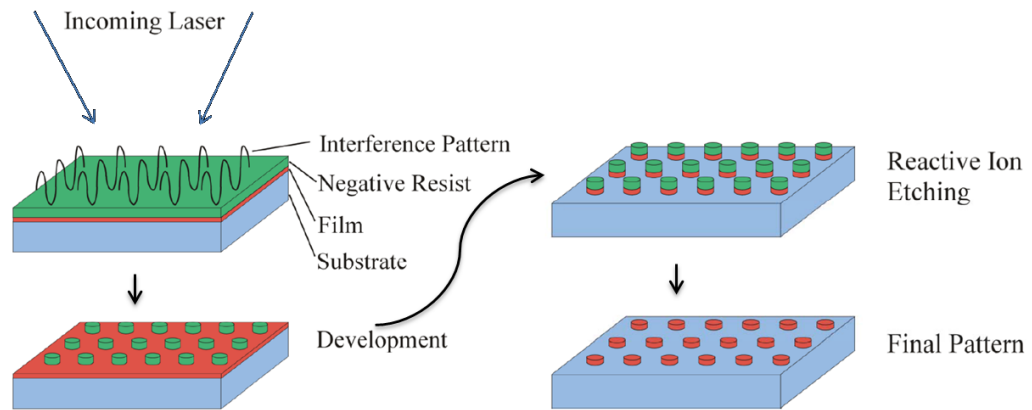
Figure 3.7: Schematic illustration of interference lithography.

3.2 Self Assembly of Nanostructures

Self assembly of nanostructures is a promising method for large area fabrication of nanostructures with low cost and effort. Approaches up to now focuses on the use of colloidal nanoparticle solutions to decorate surfaces with self assembled colloidal particles. Usage of colloids for surface structuring is called colloidal lithography. Colloidal lithography found its deserved value in nanotechnology only in recent years. Advances in the area have increased the variety of practical methods. Advancements in the synthesis methods make it possible to easily obtain highly monodisperse and dense particles with a variety of shapes and materials economically with various sizes. Colloidal lithography is a fast, cost effective way to fabricate nanoscale devices [61, 62, 63].

Colloidal lithography is based on the deposition of colloids to surfaces. Deposited colloids can be used as the final structures, they also can be used as a sacrificial or permanent masks for the deposition of final structures (like photoresist in some controlled approaches). Spherical particles can be deposited to the surface either close packed or non-close packed, there are several methods to obtain both with precision and speed. To understand colloidal deposition more thoroughly, a quick examination of effective forces defining stability of colloidal solutions is given in the next subsection.

25

3.2.1 Colloidal Dynamics in an Aqueous Solutions

Colloidal particles generally synthesized and used in aqueous solutions. Dynamics of an aqueous colloidal system is governed by two main kinds of forces. That are van der Waals attractive forces and electrostatic repulsive forces.

Intermolecular dipole attractions of molecules at short distances are called van der Waals forces. Three types of individual van der Waals dipole potentials are Keesom, Debye and London potentials. All three are inversely proportional to the sixth power of distance and can be added to obtain total van der Waals interaction potential;

$$U_{vdW} = -\frac{C}{d^6} \tag{3.1}$$

where C is the constant of proportionality that contains all three individual contributions [64, 63].

Charged surfaces that occur either by chemical manipulation of the surface properties, adsorption of ions or by dissociation of surface groups, brings electrostatic repulsion to colloidal solutions that keeps particles from coagulation. Nature of the electrostatic forces in colloidal solutions is best described with Stern double layer theory [63]. According to Stern double layer theory, the vicinity charged colloidal surfaces are covered with a rigid counter ions called Stern layer, and a diffuse layer with non-bound ions as distance gets larger. The surface potential is inversely proportional with the distance at Stern layer until it reaches the Stern potential (ψ_0), while it exponentially decays at diffuse layer as distance gets higher (Figure 3.8).
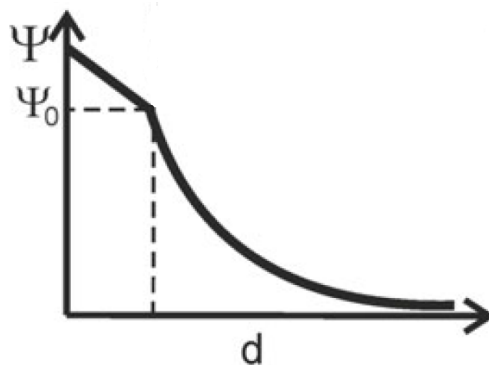
Figure 3.8: Electrostatic potential (ψ) versus distance diagram according to Stern model of electric double layer.

DLVO theory combines these two forces at work into one basic theory of colloidal stability , Total interaction potential is obtained by adding individual potentials:

$$U_{DLVO}(d) = U_{vdW}(d) + \psi(d) + U_{Born}(d) \qquad (3.2)$$
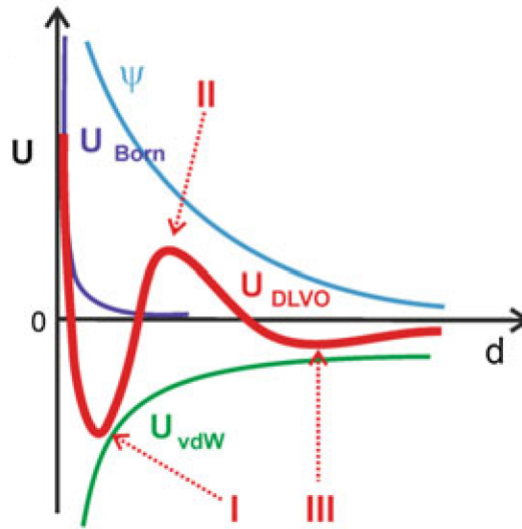
Figure 3.9: Total interaction potential of two spherical colloids in an aquaeus solution as a sum of individual contributions according to DLVO theory (Red line) [63].

Total interaction potential of two equal spherical colloidal particles according to DLVO theory is shown in Figure *3.9.* Born repulsion U_{born} is dominant at very small distances that prevents particles from overlapping. A minimum is observed at small distances because of the strong van der Waals forces (I). This primary minimum means irreversible coagulation of two particles in terms of colloidal stability. If electrostatic repulsion is strong enough, a maximum is induced at higher distances (II). The height of this energy barrier, defined by the electrostatic potential strength and electrolyte concentration in the solution is the main factor determining stability of the colloidal solutions dispersion. And finally a secondary minimum is observed at larger distances (III). The second minimum is referred as flocculation and it is reversible.

3.2.2 Close packed deposition of colloids

Close packed deposition of spherical particles can be used to fabricate highly ordered periodic structures over large areas. Deposition can be achieved by several ways .

Controlled evaporation is one of the easiest method for generating close packed colloidal monolayers. In the simplest case, a drop of colloidal solution is dripped onto the surface to be coated, after evaporation of solvent, close packed colloidal monolayers are obtained. When the liquid film evaporates, colloidal particles gets dragged to each other by capillary forces (Figure 3.10). Vertical deposition is another method for deposition of closely packed monolayers on the surface. It works by a slow vertical withdrawal of pre dipped substrate from a dense colloidal solution. Vertical deposition is method is also known as Langmuir Blodget method. The colloids proceeds to drying front and forms crystalline structure on the substrate surface (Figure3.11). Spin coating is also observed to be possible, which employs faster evaporation rates. electrostatic and electrophoretic deposition methods that uses electrostatic forces to deposit monolayers, used by several groups with success. In electrostatic deposition a pre charged surface is used to attract colloids inside the solution while electrophoretic deposition uses conductive substrates as electrolytes to induce electrostatic assembly [65].
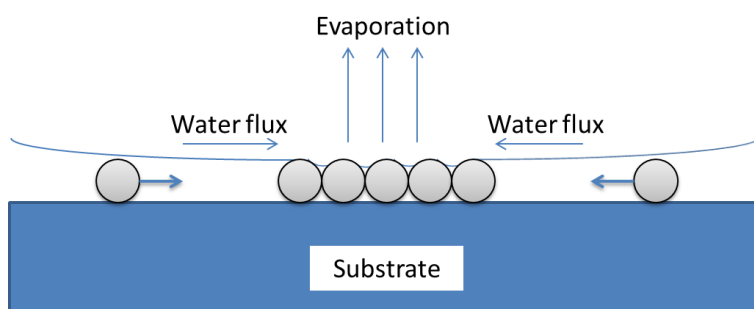
Figure 3.10: Illustration of controlled evaporation method.

Nanosphere lithography is one of the most exercised colloidal lithography methods, uses self assembly of close packed colloidal monolayers on the surfaces, by evaporation through the empty spaces and removal of nanoparticles highly ordered nanostructures can be fabricated over large areas with desired sizes (Figure 3.12).

28
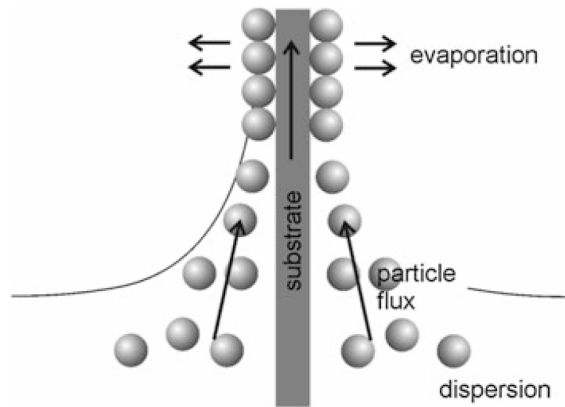
Figure 3.11: Illustration of vertical deposition method.
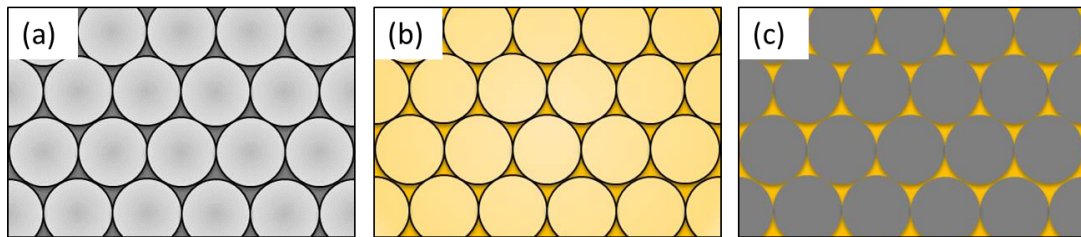
Figure 3.12: Illustration of nanosphere lithography to obtain hexagonal crystal structures (a) Nanosphere deposition (b) Material deposition (c) Surface after removal of the nanospheres.

3.2.3 Non-close packed Deposition of Colloids

Non-periodic monolayer deposition can easily be achieved by the help of electrostatic forces. Since the surfaces of colloidal particles are charged an opposite charge on the surface makes particles to adhere to the surface, while repulsive electrostatic forces between them keeps them apart. After this kind of deposition, surfaces are left with randomly deposited, non-periodic and isolated particles. This deposition method used in the experiments conducted for this thesis because of its effectiveness and ease. Since periodic non-close packed deposition is relevant with this thesis, several methods will be discussed since one of these methods can be employed, as well for periodic structure fabrication using hole mask colloidal lithography.

Non-close packed periodic sphere deposition can be divided into two approaches, using close packed monolayers and direct deposition. Isotropic size reduction [66, 67, 68] and expanding an elastomeric substrate [69, 70] are the two successfully

employed methods using closely packed monolayers for obtaining non-close packed monolayers (Figure 3.13).
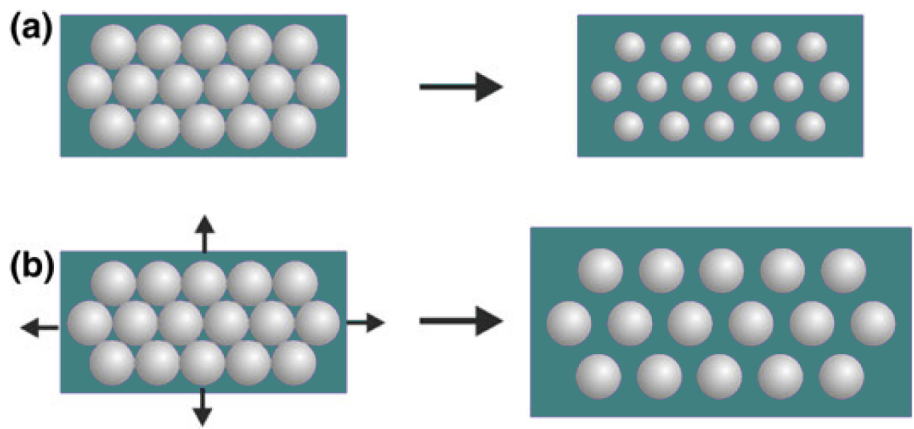
Figure 3.13: Generation of non-close packed monolayers from close-packed arrangements. (a) Plasma-assisted size reduction (b) Stretching of an elastomeric substrate.
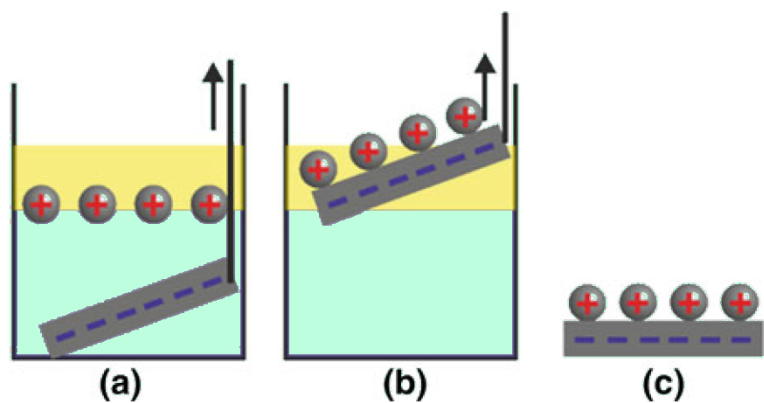
Figure 3.14: Transfer of non-close-packed monolayers from the hexane-water interface to solid substrates. (a) Assembly of colloids at the interface (b) Vertical removal of immersed substrate with a slight angle (c) Resulting non-close-packed monolayer on the solid substrate.

Spin coating of non-close packed periodic monolayers is possible by with several chemical steps, using macroporous Polymer Membranes [71].

Another method that can be used is interface coating. When nanosphere solution is slowly put in an oil-water interface, the particles are trapped in two dimensional interface (Figure 3.14). Particle density can be decreased or increased, every time preserving a constant interparticle distance of particles from each other. Then pre dipped oppositely charged angled sample is pulled out very slowly. When the sample

passes through the interface, trapped particles adheres and fixes to the surface of the sample, preserving their periodic fashion [72, 73].

A brief comparison of common surface nanostructuring methods is given in Table 3.1. As it seems HMCL is strong in almost every comparison criteria.

Table3.1: A comparison of common micro and nano structuring methods and HMCL. Comparison includes; range of , minimum feature size, structure variety and cost of the system .

Lithography	Area	Resolution	Variety & Authenticity	Cost
Direct Laser Writing (DLW)	Moderate (mm's)	Sub μm	Very High (even 3D structuring possible)	Moderate
Electron Beam Lithography (EBL)	Low (Few Hundreds of μm's)	several nm's	High	High
Focused Ion Beam Lithography (FIBL)	Low (Few Hundreds of μm's)	several tens of nm's	High	High
Scanning Probe Lithography (SPL)	Very low (nm's to μm)	Molecular	Very High	High
UV&DUV Photolithography	Large (cm's)	$\geq$200 nm	Limited (bound to other methods)	Low
Extreme UV Photolithography	Large (cm's)	Several tens of nm's	Limited (bound to other methods)	High
Nanoimprint Lithography	Large (cm's)	nm's	Limited (bound to other methods)	Low
Interference Lithography	Large (cm's)	100 nm	Moderate (only interference patterns of two or more beams)	Moderate
Colloidal Lithography	Very large (10s of cm's)	nm's	Low (only several geometries possible)	Very low
Hole Mask Colloidal Lithography	**Very large (10s of cm's)**	**nm's**	**Very High**	**Very low**

CHAPTER 4

HOLE MASK COLLOIDAL LITHOGRAPHY

4.1   A Hybrid Technique

Colloidal term in hole mask colloidal lithography (HMCL), suggest that it is a type of colloidal lithography. It takes advantage of easy deposition of spherical nanoparticles over large areas. Isolated non-close packed random deposition of colloidal spheres can easily be applied to large areas with controllable surface coverages. Colloidal part in HMCL only determines the places of the *hole masks* on the surface. Hole mask part of HMCL on the other hand, is a novel method that takes advantage of highly directional nature of thermal evaporation. In thermal evaporation materials deposited isotropically such that the deposition nature can be visualized like light emitted from a point like source. As any non-transparent object in the way will block the light and generate a shadow behind, material evaporation can be shadowed the same way. A mask that placed a known distance away from the surface shadows some parts of the surface from coating, the distances of source to hole mask and hole mask to substrate are not comparable such that deposition can be viewed as parallel coming from a distant source. When an constant angle is introduced between surface normal vector and evaporation direction, deposition position can be controlled. After removal of the mask, if the angle kept constant, surfaces are left with cylindrical particles or disks with the same diameter as holes at desired places on the surface (Figure 4.1).

Extended control over x-y plane geometrical freedom can be obtained by giving the sample holder ability to rotate in situ with material evaporation. One can consider two independent geometries to easily comprehend structural variety and limitations.
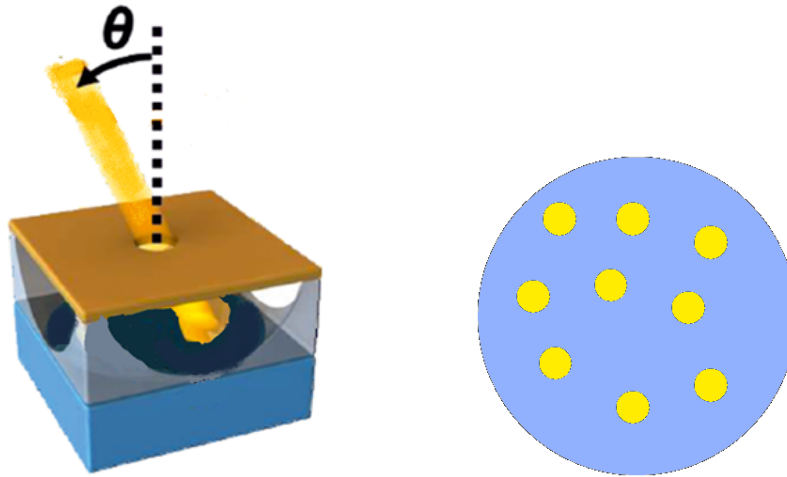
Figure 4.1: Right: Angled deposition through hole mask, Left: Position of evaporated disk through the hole can be precisely controlled

Azimuthal and polar angled deposition geometries are the two possible geometries (Figure 4.2). Structures with this method can be fabricated with any of these geometries and their combinations.
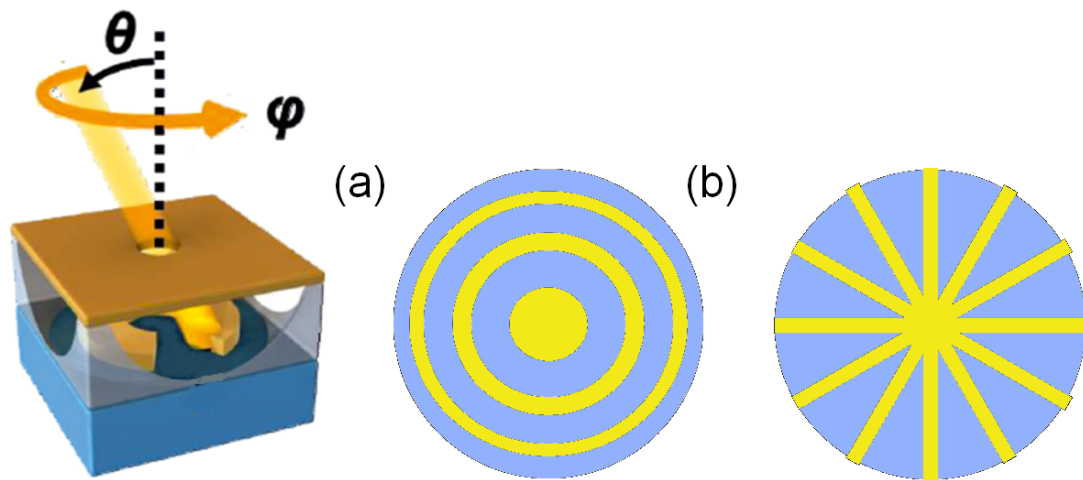
Figure 4.2: Freedom of HMCL in x-y plane with rotating angled deposition (a) polar angle geometries (b) azimuthal angle geometries

One obvious advantage of HMCL is its freedom on thickness of structure. Since evaporation thickness is highly controllable and monitorable (in angstrom scale) Desired part of structure can be thinner or thicker compared to other parts. This delicate z-axis freedom gives HMCL expanded geometrical possibilities. Moreover clogging effect makes holes smaller as material deposited through them, making smaller feature sizes

possible. Some structures fabricated with HMCL by taking 3D control and exploring clogging effect by Zhao et al. is shown in Figure 4.3.
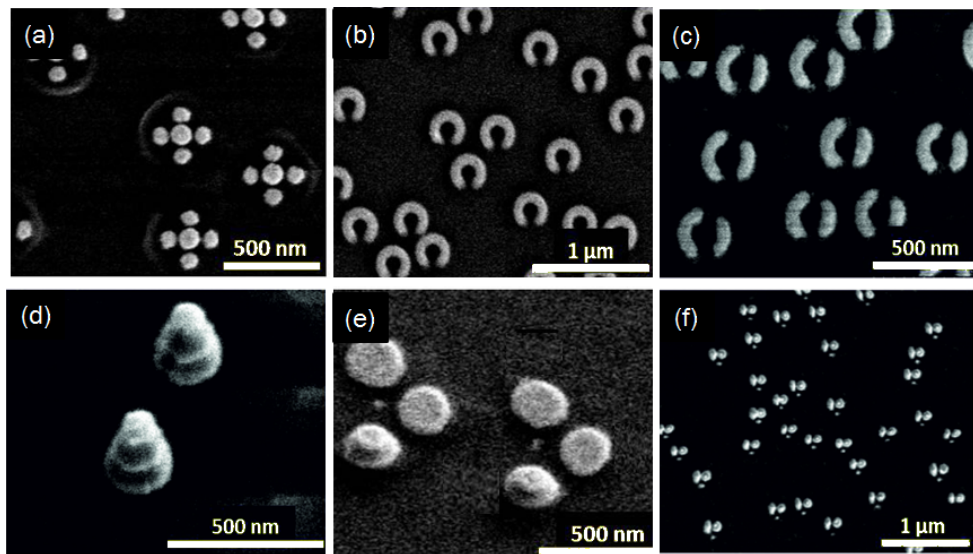
Figure 4.3: A variety nanostructures fabricated with HMCL. (a) pentamers (b) and (c) Oval structures (d),(e) and (f) Structures generated by making use of clogging effect. Adopted from [21]

Although many lithographic methods can be used to generate the holes on the mask, colloidal lithography is the most convenient way, in term of size flexibility and large area compatibility. With recently developed synthesis technologies colloidal particles with very low size diversity and high particle densities can be found commercially with varying sizes ranging from 10 nanometers to millimeters.

HMCL takes advantage of large are structuring capabilities of colloidal approaches while keeping the ability to fabricate complex geometries with precision (Table 3.1). That is why it can be considered as a hybrid method.

To generate hole mask at a small distance away from the substrate, desired surfaces are first coated with a sacrificial layer that can be selectively etched and removed later. Thickness of this layer should be controllable and uniform over the substrate area, as structure fabrication depends on it. Polymers are preferable to be used as sacrificial layer since they can be found with a great variety of properties. After the deposition of sacrificial layer, non-close packed isolated nanospheres are decorated on the polymer surface. Aggregation should be prevented to obtain nice holes. Various colloidal deposition methods can be used for desired surface distributions.

A thin mask film deposition follows, this film must be durable when compared to sacrificial layer below. As there are particles on the surface, When the particles are removed from surface their places is left uncoated. These uncoated parts are the holes of HMCL.
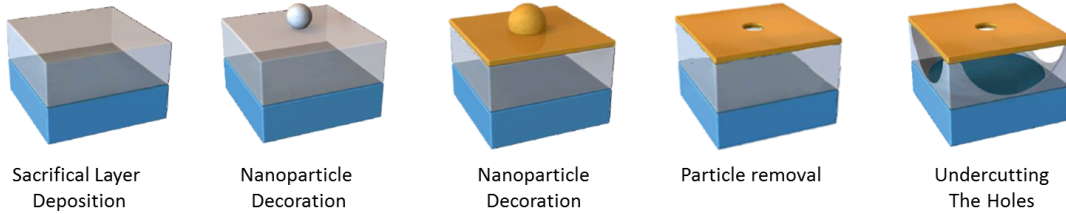
Figure 4.4: Steps for generation of hole masks

With a selective and highly controllable etch of the sacrificial film through the holes, the film can be undercutted below the holes. Holes then can be used as evaporation mask for controlled deposition of structures with angled evaporation. A schematic illustration of steps for HMCL can be seen in Figure 4.4.

4.2 Equipment and Optimized Procedure

4.2.1 Equipment

To utilize HMCL, different equipment can be used to obtain similar outcomes; for example AZ 5214 photoresist used along with PMMA in our experiments as the sacrificial middle layer; while, Zhao et al. [21], used only PMMA for same purpose. Various different colloidal nanosphere materials and sizes can also be utilized, even particles with different surface charge density and charge polarities can be optimized with polyelectrolytes. Most of the equipment that used in the experiments are readily available in GÜNAM Laboratories in METU. Several equipment (both chemicals and devices) or equivalents that are substantial for HMCL are absent, were obtained from several other laboratories in different departments owing to the friendly nature of METU professors.

Although much more variety of equipment are used for experimenting only ones that are used in successfully utilized HMCL procedure are given in the list below. Though

36

all are discussed throughout this chapter.

- Clean laboratory environment

All the experiments are conducted in a clean room environment with standart clean room devices. Moreover, some parts of the process requires yellow room lightening. Required devices include; fume hood, hot plate, ultrasonic bath and a N_2 blow gun. Also standart cleaning chemicals should be present; namely; deionized water, acetone, isopropyl alcohol, sulfuric acid (H_2SO_4), hydrogen peroxide (H_2O_2) and hydrofluoric acid (HF).

- UV mask aligner and spin coater

A standart spincoater is required to coat photoresist onto substrates. Mask aligner is only used for flood exposure of hole masked surfaces, another UV source that can large area expose AZ 5214 photoresist can also be used. In experiments *OAI model 500 mask aligner & UV exposure system* with a 500W standart *ushio* UV lamp is used. Exposure peak power is measured as 13 mJ/cm^2.

- Oxygen plasma cleaning device

Oxygen plasma cleaning device plays a crucial role in HMCL. *Femto Science: Cute plasma cleaning system* is used in experiments. Although, it is observed to be a little unreliable for undercutting the holes with high precision; this device is still one of the most essential equipment for HMCL (see section 4.3.3). This device resides in Metallurgical & Materials Engineering Department.

- Thermal evaporation vacuum chamber

Both Au film deposition and angled deposition to deposit structures are made inside a thermal evaporation chamber with a thickness monitor under vacuum (~10^{-5}torr). Tungsten evaporation boats are used to hold materials to be deposited. Boats, and highly pure materials are purchased from *Kurt J. Lesker Company*.

- Photoresist, thinner and developer

AZ 5214 Photoresist, thinner and *AZ 317 mif* developer are purchased from *Microchem.*

- Positively charged polyelectrolyte solution

Some amount of *PDDA (Poly diallydimethylammoniumchloride)* (PDAC) borrowed from chemistry department. PDDA is a positively charged polyelectrolyte with a relatively high molecular weight. It is bought from *Sigma Aldrich*, low molecular weight solution with a concentration of 20 wt% in water.

- Colloidal nanosphere solutions

750 nm *Corpuscular* brand silicon dioxide carboxyl functionalized and 262 nm *Ted Pella inc.* brand polystyrene nanoparticles worked well with this procedure. 750 nm nanosphere solution density declared as 2.5 wt% solid in its spec sheet, while 262 nm spheres declared as 1.4×10^{11} a particles per cc of solution, which corresponds to a solid content of 0.13 wt% in water.

4.2.2 Procedure

Procedure below is prepared for silicon (Si) substrates. One side polished Si wafers with arbitrary doping and crystal direction are used. With some preparation glass substrates can also be used (silanization to be precise). Usage of glass substrates is discussed in next sections.

1. Cleaning the substrates

   Cleaning of samples is important for the proceeding processes to be successful. Cleaning consists of the usual 3-solvent cleaning subsequently with DI water, acetone and isopropyl alcohol in an ultrasonic bath for 10 minutes respectively. Then the samples were dipped in piranha solution (3:1; $H_2SO_4 : H_2O_2$) for more than 15 minutes under a fume hood to eliminate any organic residues. Si

samples are dipped in 10% HF solution to remove SiO_2 layer, which renders the surface of the wafers highly hydrophobic to enhance photoresist adhesion.

2. Photoresist Coating

Thickness of this layer is deposited to be twice of used colloidal particle diameter; $\frac{1}{2}$ particle diameter to resist thickness ratio well fits for desired amount of undercutting and angled deposition with reasonable angle values. Clean samples were coated with AZ 5214 photoresist using a spin coater. Its thinner is required to have extra control over the thickness since undiluted AZ 5214 photoresist is designed to form about 1.5 μm thick films. Thinner is used to form layers with 580 nm film thicknesses. 580 nm is preferred instead of 530 nm to obtain $\frac{1}{2}$ particle diameter to film thickness ratio because of the denting effect that will be discussed later. 1500 nm resist thickness is achieved by spin coating undiluted photoresist at 3900 rpm spin speed; while, 580 nm film thickness achieved by spin coating $\frac{2}{3}$ diluted resist at 4100 rpm. Deposition carried by dripping of photoresist to surface until it covers the whole surface. Spin coater programmed to reach desired speed with high acceleration, hold constant speed for 45 seconds and slow down with small deceleration. Samples were prebaked at $100°C$ for 1 minute on a hotplate for prebake. It is very important not to expose samples to any kind of UV radiation after this step until successfully completing development process.

3. Plasma treatment

Photoresist coated samples are treated with 1 minute oxygen plasma for surface hydrophilization. Figure 4.10 given in section 4.3.3 shows the difference in wettability for untreated and 1 minute oxygen plasma treated samples. Great care should be taken not to expose samples to sunlight in this step since exposure may ruin success of the procedure. Samples were carried inside aluminum foil to block any light.

4. Polyelectrolyte deposition

PDDA solution diluted with DI water to 0.2 wt% and deposited on surface by dripping the solution to the surface until the whole surface covered. Immediately after DI-water rinse and N_2 blow dry follows. Deposited PDDA density is observed to be one of the two parameters that defines the surface coverage

of particles. 0.2 wt% density well fits for experimenting, which then can be changed for desired surface coverage.
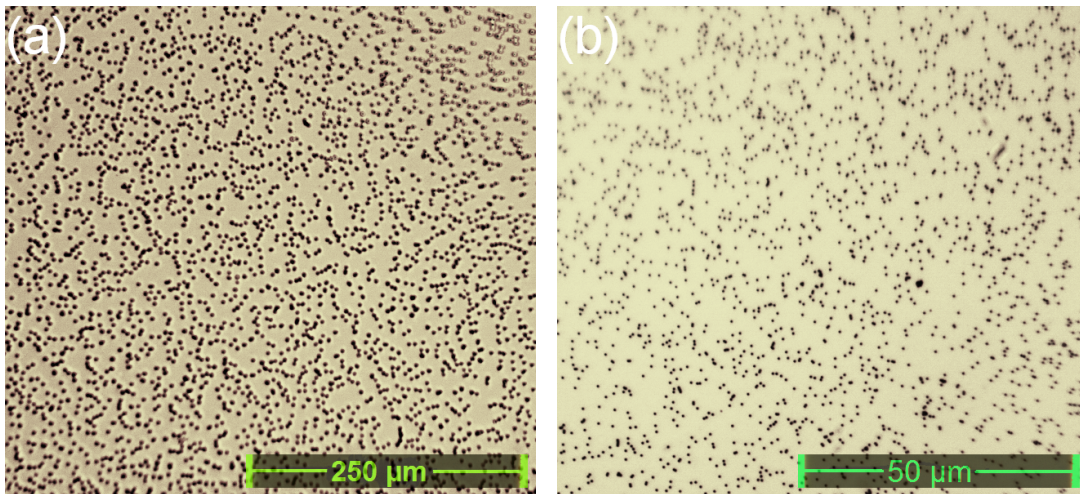
Figure 4.5: Optical microscope showing the surface coverage of nanoparticles after deposition of (a) 750 nm (b) 250 nm particles
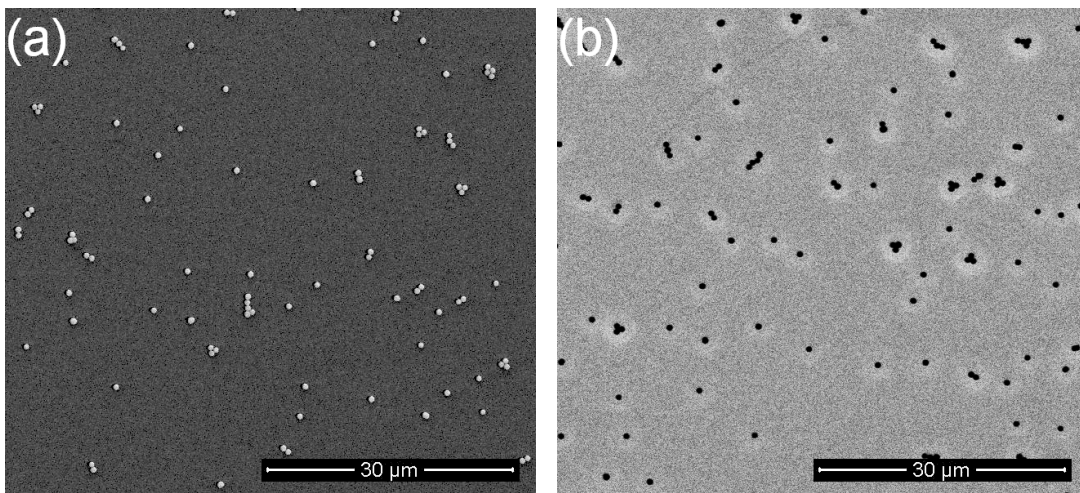
Figure 4.6: SEM images of the surface of the photoresist after 0.2 wt% PDDA and 0.125 wt% 750 nm colloidal particle deposition (a) after successful nanoparticle deposition (b) after particle removal, exposure and development

5. Particle deposition

Nanoparticle solutions are diluted with DI-water to 0.125 wt% for 750 nm and 0.026 wt% for 250 nm particle solution. Prior to coating the diluted solutions are ulrasonicated for 20 minutes to separate flocculated particles inside the colloidal solution. Solutions are then dripped onto substrate until it covers the

40
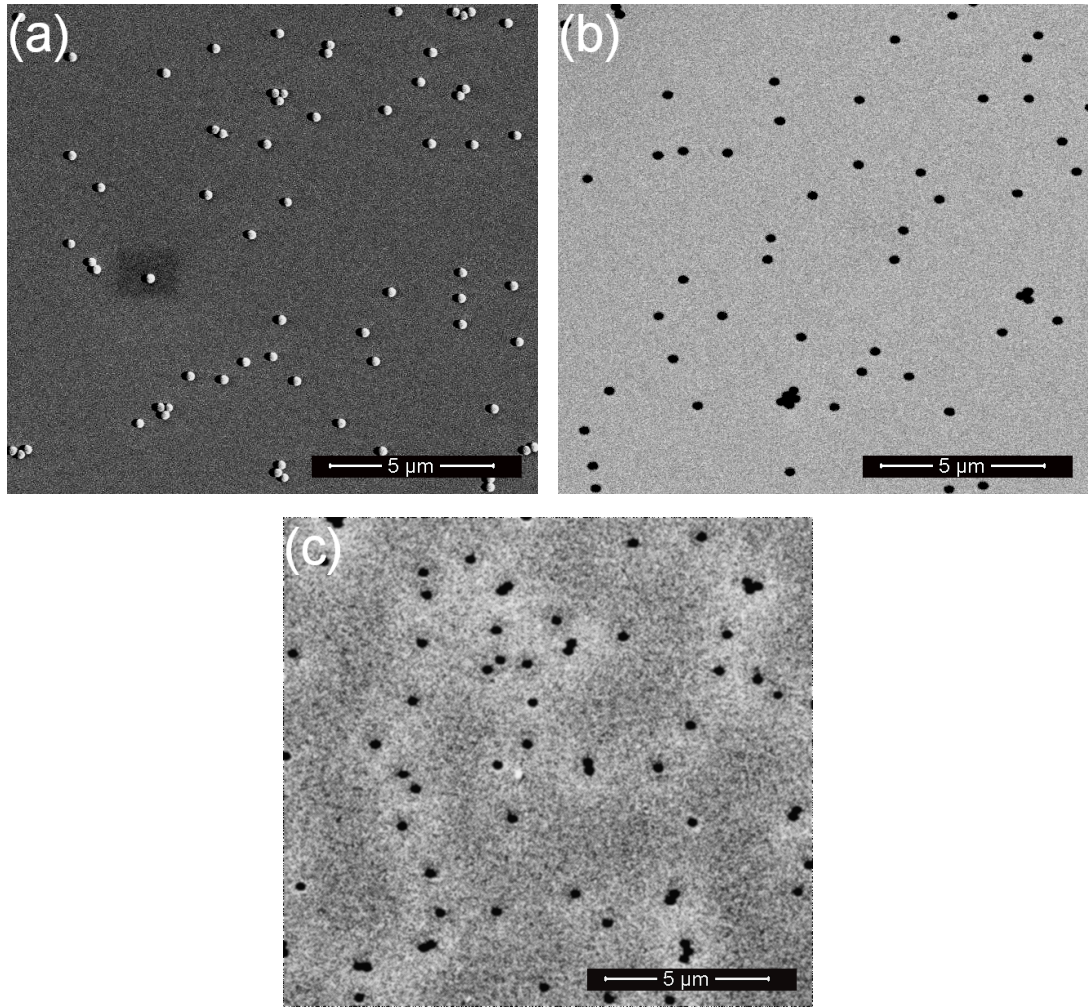
Figure 4.7: SEM images of the surface of the photoresist after 0.2 wt% PDDA and 0.013 wt% 262 nm colloidal particle deposition (a) after successful nanoparticle deposition (b) after particle removal (c) after exposure and development

surface, covered surface is left to settle for 1 minute and washed with DI water. A subsequent N_2 blow dry is applied. Nanoparticle density is the other parameter defining the surface coverage. Optical microscope picture of the surface is shown in figure 4.5 for both (a) and (b) after this step, respectively.

6. Au film deposition

   40 nm of Au film is deposited to particle decorated surface to both block UV radiation and oxygen plasma etching. It has been found that sample surfaces should be in electrical contact with sample holder in this step (see Section 4.3.6). Electrical contact is achieved by using a small piece of carbon conductive tape attached to the samples.

41

7. Nanoparticle removal

   Particles are removed from the surface by ultrasonication for 10 minutes in DI-water. After particle removal surface is left with holes on the Au film with same diameter as removed nanoparticles.

8. Exposure and development

   Samples are exposed to UV flood exposure for 10 seconds with the UV mask aligner system, then developed in AZ 317 mif developer for 2 minutes. Au film here acted as a photomask so that the exposed photoresist is removed in development. To obtain undercuts both exposure dose and development time are kept excessive. In this process most of the undercutting is done in this step, exposure and development time can be lower for undercutting with plasma etch.

9. Oxygen plasma etching

   30 min oxygen plasma session is followed both for removing remnants of photoresist left on the surface and widening the undercuts. Au film acted as oxygen plasma mask, preventing etching of Au coated parts. The oxygen plasma device operation was observed not to be very fitting for precise undercutting; probably because, it's intended purpose is solely cleaning.

If all the processes done correctly hole masks are successfully generated and the samples are ready for angled evaporation to generate desired structure geometries. Scanning electron microscope images of substrates after some steps are given in Figure 4.6 and 4.7. Detailed information and discussion about this procedure including how parameters for each step are decided will be explained in the next section. Conducted experiments with different equipment; encountered problems, solutions and tricks on each process are discussed in related subsections.

4.3   Procedure Details

Utilization of HMCL achieved by optimizing process steps explained in previous section. Most processes have some level of freedom under some minimum and maximum boundaries (ie. process time, chemical concentration and/or device properties). For some processes, these boundaries are found to be very narrow, small differences

in process details diverge into large differences on the results. When all the parameters are kept inside these boundaries HMCL is usually successful. Most of these boundaries were examined throughout the experiments and will be explained in next sections. Details about each process will be given and other possibilities that are left to be examined will be discussed. Problems, reasons and possible or definite solutions will be discussed. This section aims to be a comprehensive guide to researchers, who want to reproduce our procedure and maybe develop it. For this purpose each observation and problem is discussed throughout the sections. Each subsection is devoted on explaining details on each process step. The organization of this section is designed to be relevant with the order of process steps, experiments are not conducted within this order.

4.3.1 Glass Substrate Issue

Experiments conducted on both Si and glass substrates, with same cleaning procedure (without HF dip) glass samples yield very poor results. On particle coating step partial cracking of photoresist is observed; moreover, resist got almost completely removed in particle removal step in the ultrasonic bath. The main problem of glass is its highly hydrophilic nature, which causes poor adhesion to highly hydrophobic photoresist moreover this hydrophilic nature allows water molecules to stick to the surface even after blow drying. Any water that is left on the surface spoils photoresist adhesion. To remove sticking water molecules, glass substrates were heated at 150 °C for 2 hours to evaporate any remnant water molecules. After this process adhesion strength and stability of photoresist film was highly increased but still did not reach to required level. Samples prepared this way successfully survived particle coating step, but, partial cracks observed in ultrasonic particle removal step, and more cracking and removal is observed in development step. As a result ~75 % of the total area of samples did not survive, successful holes created on only about 25 % of the total area.

To successfully use glass substrates for large area HMCL, a more adhesive sacrificial layer may be used which requires new optimization steps; more favorably glass surfaces may be silanized prior to photoresist coating. Silanizing of glass can be done

with several silanizing agents like triethoxysilane, trimethoxysilane etc. Generally substrates are left overnight in a diluted solution of silanes to let organofunctional silane molecules to self-assembly on the surface. Silanization increases hydrophobicity, resulting in an enhanced adhesion of photoresist.

4.3.2 Sacrificial Polymer Layer

AZ 5214 photoresist is used as the sacrificial polymer layer. Thickness of the photoresist is optimized for desired $\frac{1}{2}$ particle diameter to layer thickness ratio. To optimize required thickness values spin speed and dilution of resist has been altered and resulting thickness values were measured with Dektak profilometer. Thickness measurements yield around 30 nm of deviation, measurements taken from at least 4 different positions on the sample averaged to get more reliable results. Different spin speeds and dilutions are used and to finally obtain 1500 nm for 750 nm particles and 580 nm for 262 nm particles. Measured film thickness values with several concentrations are given in Table 4.1.

Table4.1: AZ 5214 film thickness with different dilution ratios and spin speeds

	3000 rpm	3900 rpm	4000 rpm	4100 rpm
Non-diluted	2 μm	-	1.65 μm	**1.5 μm**
25 % diluted	-	-	800 nm	-
33.3 % diluted	-	**580 nm**	600 nm	-
50 % diluted	-	-	325 nm	-

After prebake at 100 °C for 1 minute, AZ5214 photoresist becomes photo active, it is crucial to keep the samples from UV exposure (eg. sunlight) until the development step. Samples should be kept in a dark environment and all possible proceeding processes should be applied in yellow room environment.

We tried PMMA (polymethyl methacrylate), a common e-beam resist, to be used as the sacrificial layer in early stages of the experiments. PMMA is intended to use for 262 nm and 91 nm particle diameters, to keep 1/2 ratio desired polymer thicknesses 530 nm and 180 nm, respectively. For this purpose, PMMA C7 (7% solids in chlorobenzene) is diluted with its solvent chlorobenzene to C5 which yields around 500 nm thickness at 2500 rpm spin speed and to C3 to obtain around 200 nm thickness

at 4000 rpm spin speed. Usage of PMMA rules out the exposure and development step since it is not sensitive to UV radiation and flood electron beam exposure is not possible with any accessible device. This means that to undercut the holes only oxygen plasma is possible.

Experiments with PMMA are not brought to the end because of some drawbacks. One drawback is that oxygen plasma undercutting is not reliable for 500 nm thick PMMA with used device (more information given on related subsection). For about 200 nm films used with 91 nm particles, undercutting should work with a long plasma sessions; however, experiments show that surface coverages with enough density is not achievable with the 91 nm nanosphere solution. Even undiluted deposition yield poor surface coverages because of highly coagulated solution. To remove coagulated particles from the colloidal solution a 200 nm filter is used, it worked but this time density of deposited particle density is observed to be even lower (Figure 4.8). Another drawback is impurities on the surface of coated PMMA film most probably caused by the old the age.
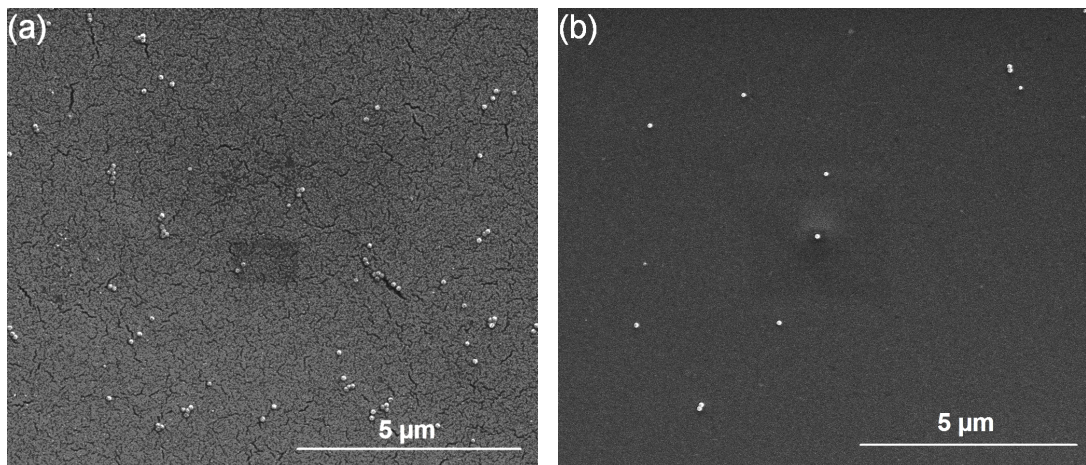
Figure 4.8: Surface coverage of 91 nm spheres on PMMA surface deposited with densest possible solutions of (a) undiluted colloidal solution (b) filtered colloidal solution

4.3.3 Oxygen Plasma Treatment

Coated samples were treated with a short oxygen plasma session. Plasma treatment renders hydrophobic polymer surface hydrophilic without changing bulk properties. increased surface wettability is important for particle deposition step. A brief treat-

ment is enough since excessive treatment durations will not contribute to surface wettability [74]. More than a minute of plasma treatment is found to be unnecessary since wettability properties does not significantly increase by longer treatment (Figure 4.9).

Oxygen plasma treatment also alters charge properties of polymer surfaces, an increased negative zeta potential is observed on PVC surfaces after plasma treatment by Khorosani et al [75]. Increased surface charging is desirable in HMCL procedure since it will catalyze polyelectrolyte deposition in the next step.
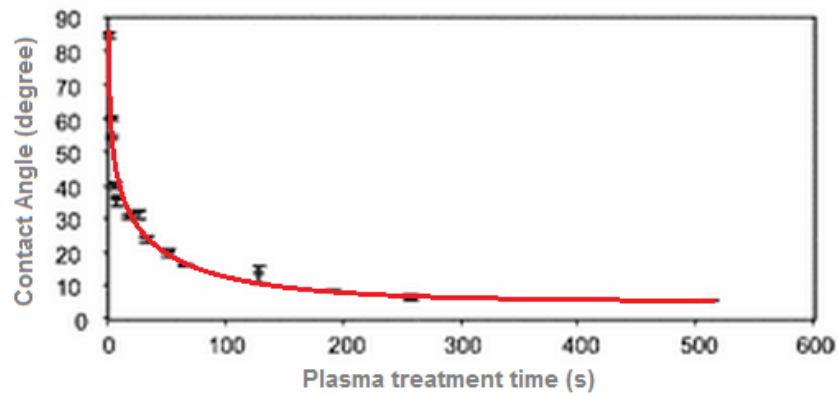
Figure 4.9: Contact angle versus plasma treatment time. Adopted from [74].

Observed wettability is better for AZ5214 photoresist than PMMA after plasma treatment.
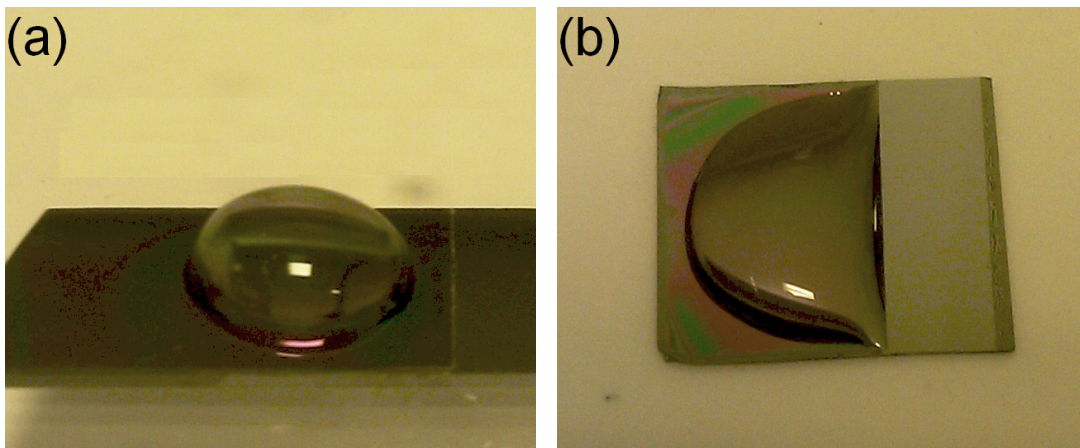
Figure 4.10: Same amount of water ($100 \mu l$) dripped onto (a) untreated and (b) 1 min oxygen plasma treated photoresist surface

4.3.4 Nanosphere Deposition

Nanoparticles can be commercially found with various sizes and chemical properties in liquid colloidal solutions or dry. For deposition of nanoparticles surface charges of both nanoparticles in solution and surface of the polymer film plays very important role on the success of deposition. Polymer surfaces are generally negatively charged, this results in negative surface charges of both the polymer and non-functionalized nanoparticles. In early stages of experiments before utilization of a positively charged polyelectrolyte middle layer, several experiments were conducted with no success for the deposition of well isolated particles on the PMMA surface. Low adherence of particles because of the repulsive electrostatic forces is the main reason behind it. Only the controlled evaporation as the colloidal deposition resulted significant surface coverage. It is conducted by a solvent drip and dry it under room conditions overnight, since all the particles in dripped solution will deposit to the surface after solvent evaporation, very dilute solutions used (on the order of 10^{-5} wt%). Controlled evaporation experiments yield poor results as very increased aggregation and discontinuous surface coverages were observed. (Figure 4.11).
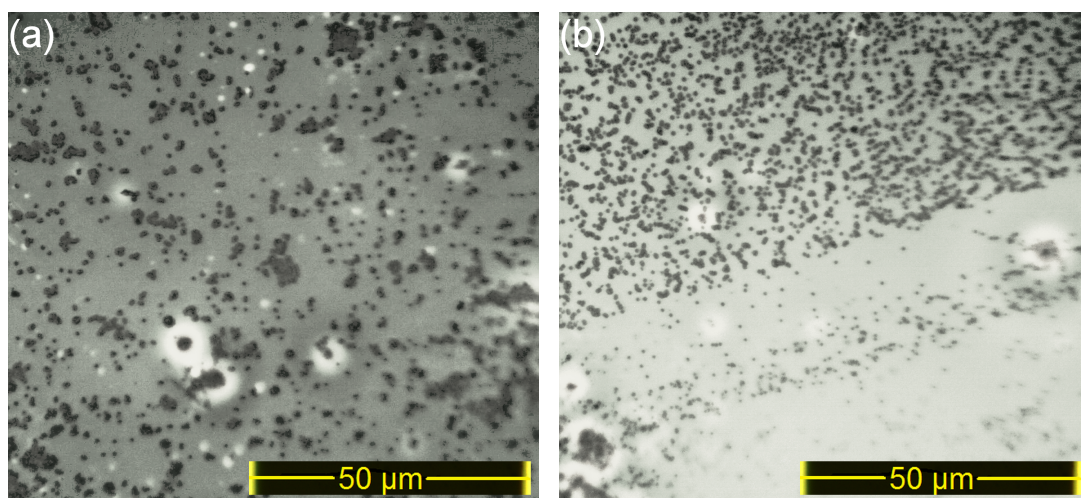
Figure 4.11: Microscope images of particles deposited on PMMA surface with dropping a very diluted solution (in the order of 10^{-5} wt%) and letting it self dry, (a) A denser solution (b) a dilute solution (10^{-5} wt%). Both show discontinuities on the surface

With a positive polyelectrolyte deposition onto the resist surface, charge polarity of the surface can be altered to become positive. This way attractive electrostatic forces between the oppositely charged resist and nanoparticle surfaces makes particle de-

position much more efficient. Particles adhere to the surface stronger making them more resistant to flow forces induced by solvent evaporation. With this information Poly(diallydimethylammoniumchloride) (PDDA) is borrowed from Dr. İrem Erel in chemistry department. PDDA is a positive relatively high molecular weight polyelectrolyte with long molecule chains; that very well fits for desired application. It is bought from Sigma Aldrich, low molecular weight version with a concentration of 20% wt in water. Deposition conducted by dripping a diluted polyelectrolyte solution to the surface until whole surface is covered. Immediately after samples are rinsed in DI-water and N_2 blow dried. Several experiments with different dilution rates are made, and well distributed surfaces are obtained. Effect of PDDA density to surface coverage of deposited nanoparticles is observed. (Figure 4.12). 0.2 wt% PDDA density is chosen for procedure because it well fits for desired preliminary applications.
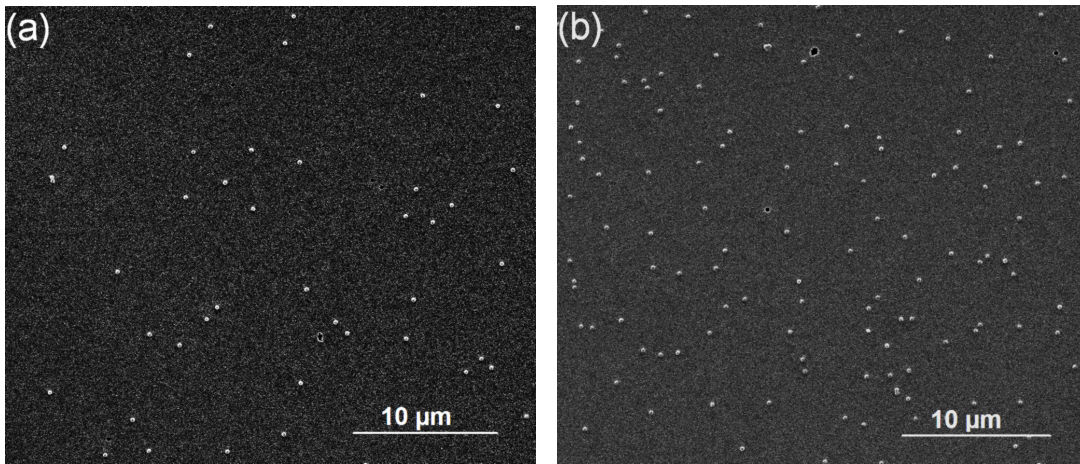
Figure 4.12: Effect of PDDA concentration on surface coverage of particles (a) 0.05 wt% (b) 0.2 wt% PDDA with fixed particle density of 0.026 wt% of 262 nm nanospheres

Experiments conducted with colloidal solutions of; 750 nm Corpuscular brand silicon dioxide, 262 nm Ted Pella brand polystyrene and 91 nm Ted Pella brand polystyrene nanospheres. 750 nm nanosphere solution density declared as 2.5% solid in its spec sheet, while 262 nm spheres declared as 1.4×10^{11} particles per cc of solution which corresponds to 0.13 wt% of mass fraction. Effect of particle density to surface coverage is examined (Figure 4.13 and 4.14)
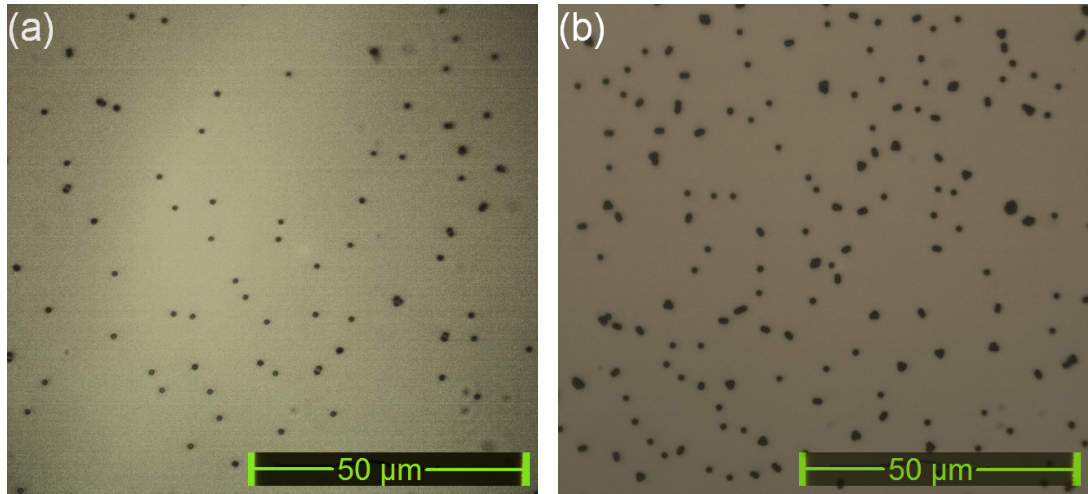
Figure 4.13: 750 nm particle surface coverage with fixed PDDA 0.2 wt% (a) 0.125 wt % (b) 0.25 wt%
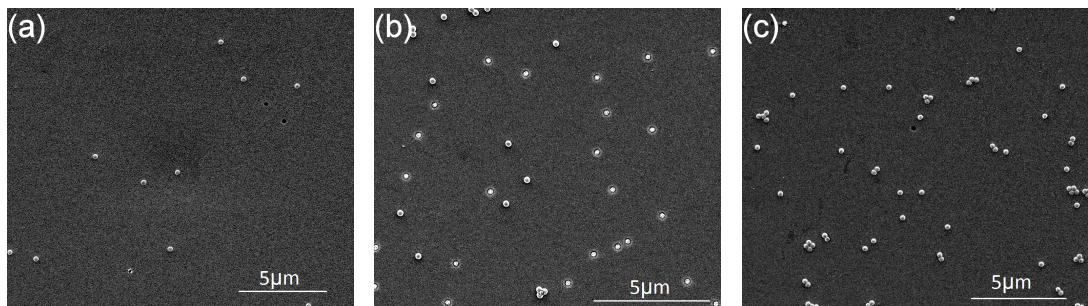
Figure 4.14: Effect of varying particle density on surface coverage with fixed PDDA density of 0.2 wt% for 262 nm particle deposition (a) 0.013 wt% (b) 0.026 wt% (c) 0.052 wt% particle mass fractions.

4.3.5 Metal Film Deposition

After nanospheres are successfully deposited on samples a thin Au film of 40 nm thickness is deposited on the surface to mask UV radiation and oxygen plasma's etching effects. Deposition made in a vacuum thermal evaporation chamber.

Optimization of thickness was a little more cumbersome than the previous steps. Smaller than 40 nm thicknesses of Au film observed that it does not efficiently block UV radiation resulting destruction of hole masks by solution of whole photoresist in the developer.

Some experiments with Ag instead of Au is conducted, Nevertheless; it is good for masking UV radiation, Ag is not a good mask for oxygen plasma. In oxygen plasma step Ag film is observed to oxidize very fast and surface of the film cracked and

peeled (figure 4.15). For now Au seems to be the best option for this layer.
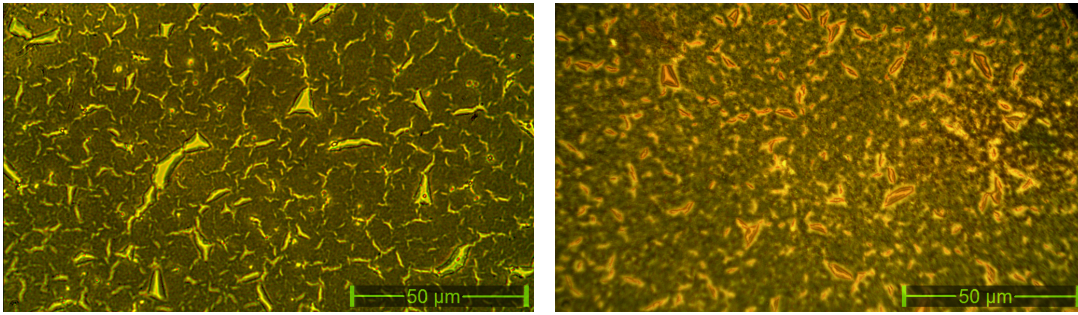
Figure 4.15: Damaged Ag surface (a) after 20 minutes (b) after 30 minutes of plasma etching

4.3.6   Premature Separation

After Au film deposition, reduced surface coverage densities are observed. Further examination of samples under atomic force microscopy (AFM) revealed that nano particles leave the surface during thermal evaporation process leaving the surface with blocked half-holes that are no good for HMCL because neither developer nor oxygen plasma can penetrate the Au film (figure 4.16 and 4.17). We call this phenomena premature separation of nanospheres.
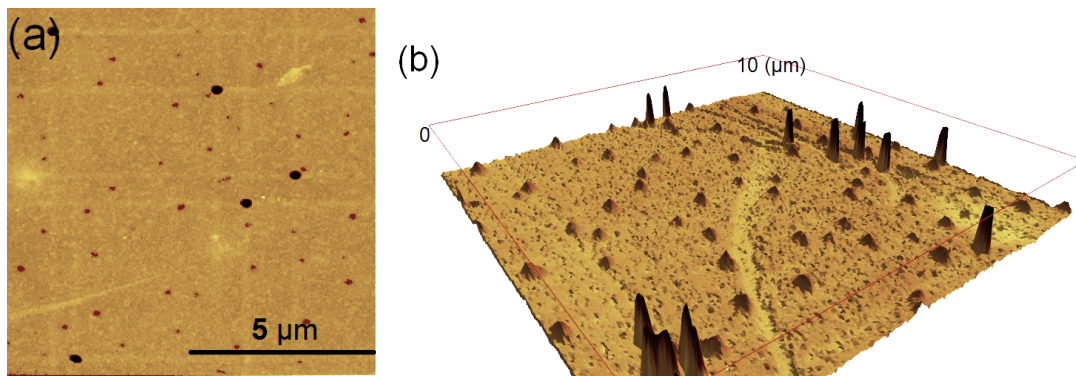
Figure 4.16: (a) AFM image of substrates after Au deposition (b) upside down 3-D view of another afm image

After some thought and research on the possible reason or reasons behind premature separation, the charging of evaporated Au film is found to be the reason [76]. Since particles are charged too there can be a repulsive force that makes particles leave the surface prematurely. In *figure* 4.16 (b) the depth of holes resulted by premature separation seems to be in a small range and in figure 4.17 the depth of unsuccessful
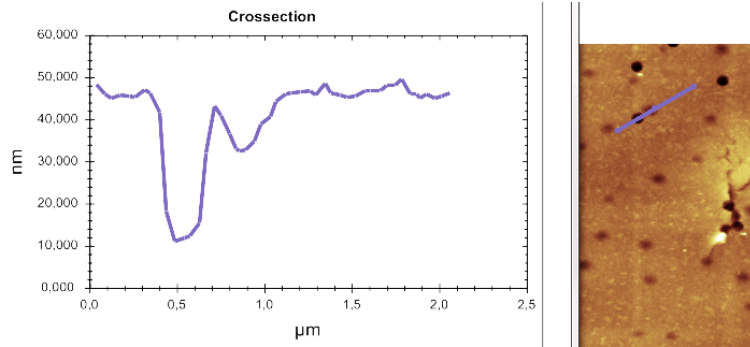
Figure 4.17: AFM crossection of a successful hole and a nearby failed hole caused by premature separation

holes is around 6 - 10 nm, this means that most of the particles are left the surface on early stages of evaporation.

Premature separation is prevented by grounding sample surfaces to sample holder in evaporation chamber, a conductive carbon tape is used to make sure surface of samples are in electrical contact with the sample holder.

4.3.7 Nanoparticle Removal

After a successful deposition of Au film onto the nanosphere deposited photoresist surfaces, nanoparticles now should be removed to leave holes on the surface of the Au film. An ultrasonic bath in DI water for 10 minutes is found to be enough for this purpose for any of the three sizes of particles. Removals made in a floating petri dish on a water filled ultrasonic bath. Experiments conducted for different times of this step. Even 2 minutes seems to be enough to remove 750 nm particles since they are more vulnerable to liquid flow forces due to their size; however, 262 nm and 91 nm particles may stick stronger. 10 minutes ultrasonic bath observed to successfully work with all three of particle sizes. 4.6 and 4.7

4.3.8 Plasma Etching

Plasma etching of undercuts has already been found to be a successful way for HMCL [22, 21]. Early experiments are also conducted with the usage of only PMMA as
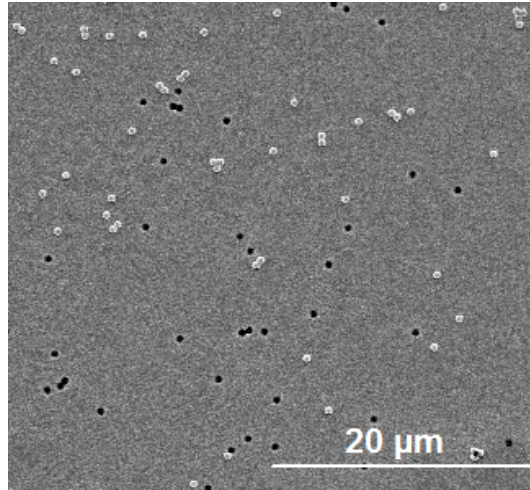
Figure 4.18: Partially removed 262 nm particles ofter 2 minutes of ultrasonic bath

the sacrificial layer with only plasma etching to undercut the holes. However, the oxygen plasma device used in metallurgical department by permission by Dr. Emrah Ünalan is designed for cleaning purposes, and is not found to be fitting for large depth undercutting. Etch rates are found to be very low, and long processes yield uneven etch depths with same etching time. After these observations the device is decided to be not fitting for the undercutting purpose. Instead a long oxygen plasma etching is applied at the readily undercutted holes, to clean any resist residues from the surface, and widen the undercuts a little bit.

4.3.9 Exposure and Development

Inefficiency of oxygen plasma device for etching thick films (>200 nm) make it necessary to find another method for undercutting the holes. For this purpose exposure and development of a photoresist is fitting, as the hole mask can also be used as a photolithography mask that is ready on the surface, photoresist is illuminated through these holes. Even wide undercuts achieved with over exposure and over development.

Undercuts generated on glass surfaces with with 750 nm particle size are examined with a back illumination optical microscope. 5 sec flood exposure (60 mJ/cm2) and 1 minute of development in AZ 317 mif developer that is the standart procedure of the AZ 5214 resist recommended by the producer yield poor undercuts. For deeper undercutting both steps are doubled to 10 sec exposure and 2 minutes development

which resulted better undercuts (figure 4.19).
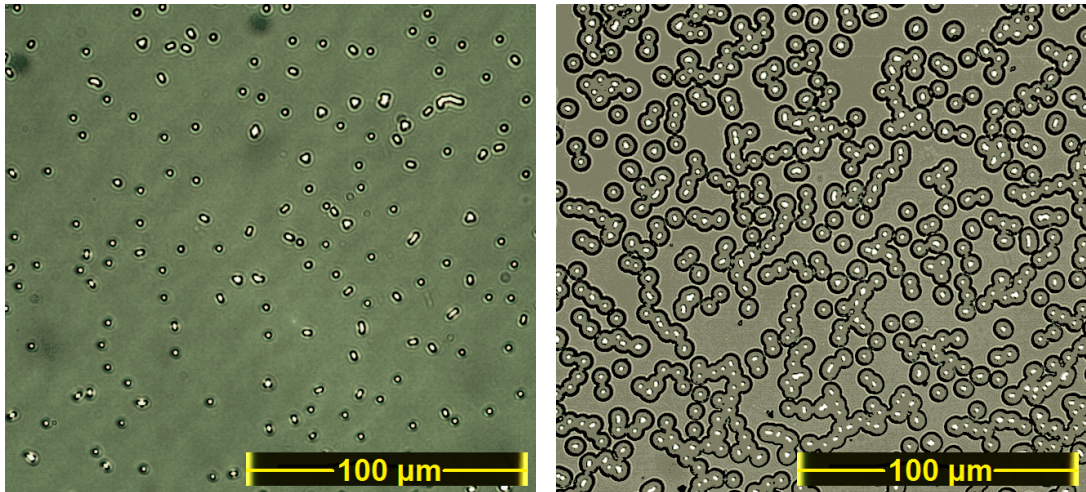
Figure 4.19: Back illumination microscope pictures of glass substrates decorated with with 750 nm holes. Left: 1 min development and Right: 2 minutes development applied.

4.3.10   Uneven Undercutting

Although, well undercuts are achieved with 750 nm hole diameter with over exposure and over development, usage of 262 nm holes with the same procedure is not as successful bringing out new issues. One of these issues is uneven undercutting. Some 262 nm holes are well undercutted while some of them are observed to very briefly undercutted of not undercutted at all (figure 4.20). This issue prevents successful usage of some holes in angled evaporation step and consequently lowers the overall surface coverage of evaporated structures.

Uneven undercutting is on some level solved by increased development time (3 minutes) (Figure 4.21). However very big undercuts may increase denting of holes that is discussed in the next subsection.

4.3.11   Denting of Holes

Denting of holes is another issue associated with undercutting with over exposure and over development. Some denting is observed around the holes. This effect yields important control problems for 262 nm holes, since depth of the dents are different
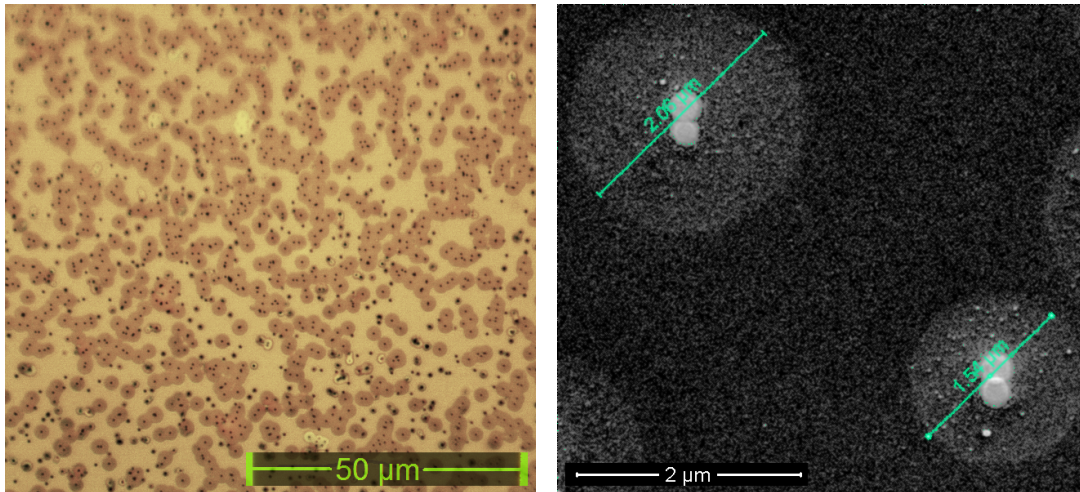
Figure 4.20: Uneven undercuts are observed with 262 nm holes, after over exposure and over development. Left: Optical microscope picture of Au film surface, right: SEM picture after particle deposition.

from hole to hole because of uneven undercutting 4.22.

Larger dents are observed around close distanced holes, this means that large undercutting until two independent undercuts merge results an enhanced denting on the surface, that makes material deposition even more unreliable. as dent depths can reach up to 100 nm. The control problems associated with denting of holes is error on evaporation position, If all the dents are nearly equal in depth, like it is for 750 nm holes, denting is not a big concern because the polymer thickness or evaporation angle can be altered to overcome it. however uneven denting observed on 262 nm holes, since the evaporation position will be different for different structures, lowers the credibility of HMCL. Figure 4.23 shows dimer distance variations caused by uneven denting.

that uneven denting resulted varying inter-particle distances between individual particles. Inter particle distance of the dimer on the right side seems to be bigger because of less denting on that hole.

Denting effect is probably associated with the forces occurring during the evaporation of developer. No dent is expected on a completely oxygen plasma etched hole masks. Increasing the development time to generate undercuts from all the holes resulted enhanced denting of the surface. There seems to be a trade off here, either loose
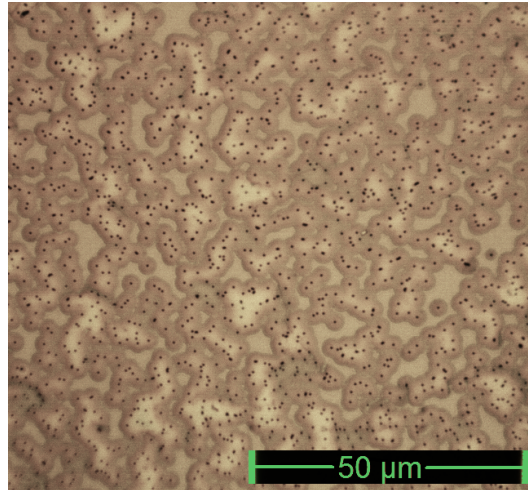
Figure 4.21: Optical miscroscope picture of 3 minutes developed sample with 262 nm holes.

some of surface coverage or reliability of angled deposition. This trade off should be considered according to requirement.
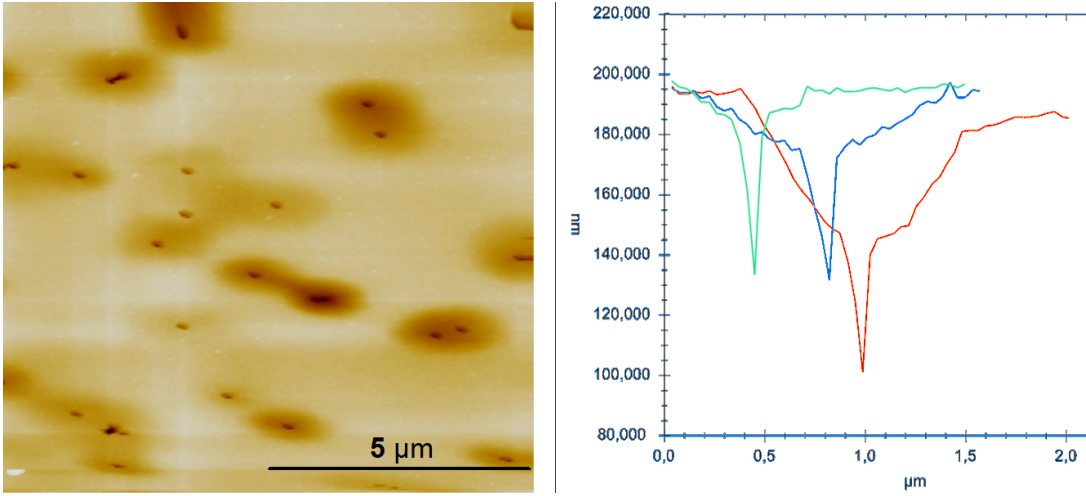
Figure 4.22: Denting of holes are observed with 262 nm holes, after over exposure and over development, uneven dent depths can be seen in the AFM crossection graph each color are taken from different holes (Right)
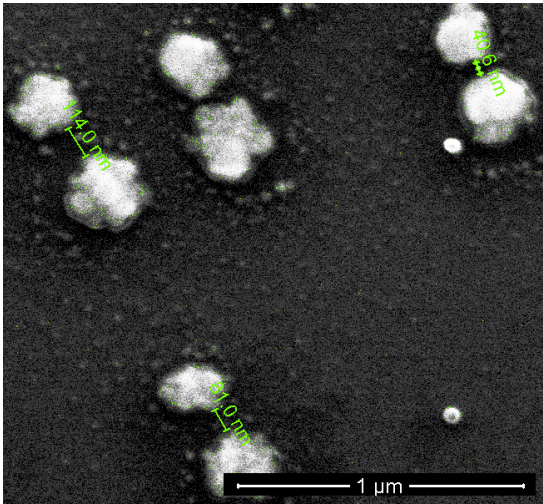
Figure 4.23: Uneven denting caused variations on interparticle distances of individual dimers

4.4 Angled Deposition

4.4.1 Sample Holder Modifications

Sample holder inside the vacuum chamber should be modified for angled deposition. To observe undercutted width under the holes and to fabricate some simple structures consisting of multiple metal nano-disks; a simple sample holder is fabricated in machine laboratories of METU Physics Department. Holder designed to hold samples at a constant azimuthal angle during the evaporation process. A rotatable disk added to manually rotate the holder in polar direction to perform multiple evaporation steps conveniently (Figure 4.24).
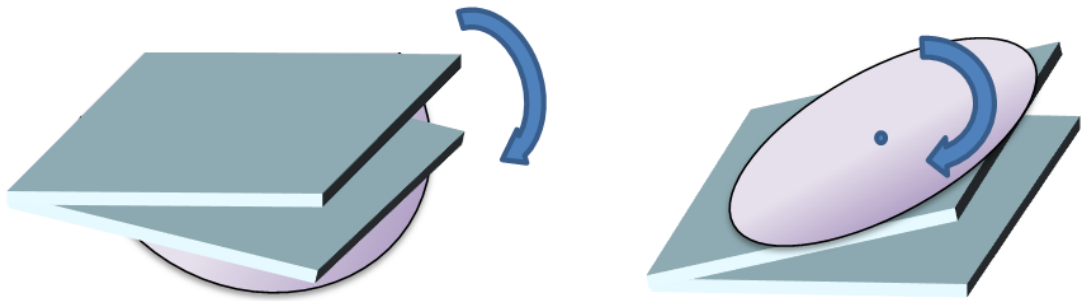
Figure 4.24: Simple angled evaporation sample holder.

For dimers the angle of deposition for obtaining dimers with desired side to side distance *a is calculated by;*

$$\theta = tan^{-1} \left(\frac{d+a}{2t} \right)$$

where *d* is the hole diameter and *t* is the polymer film thickness.

4.4.2 Preliminary Structures

Preliminary dimer, trimer and quadromer structures fabricated on large areas with 750 nm feature diameter. Ag is used as the deposited material, thickness of the structure kept at 40 nm solely for imaging purposes. Well separated structures achieved by evaporation with calculated angle. Dimers are excluded from figures since there are a lot of dimers in next subsections.
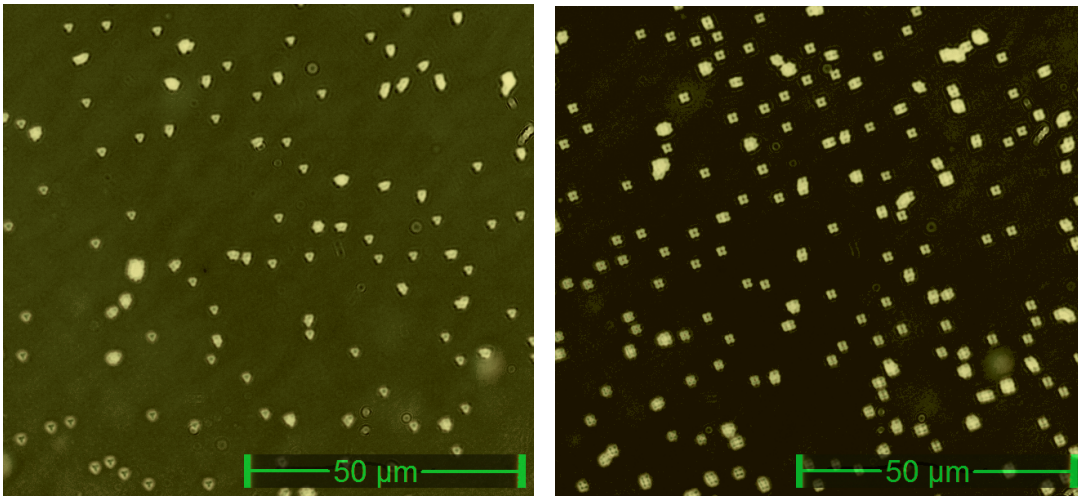
Figure 4.25: Optical microscope pictures of preliminery structures that are fabricated by several consecutive angled evaporation sessions through 750 nm holes. (a) Trimers, (b) Quadromers.
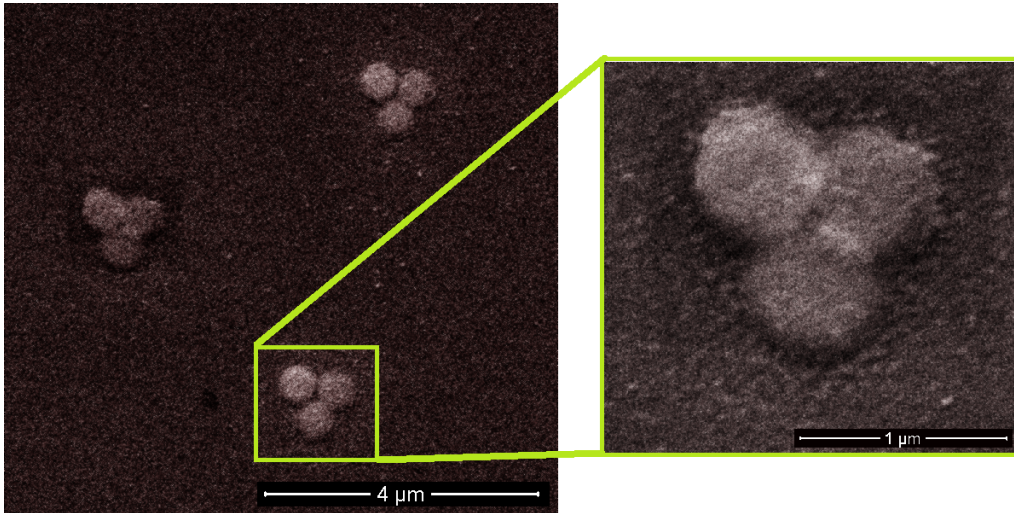
Figure 4.26: SEM pictures of 750 nm trimer structures
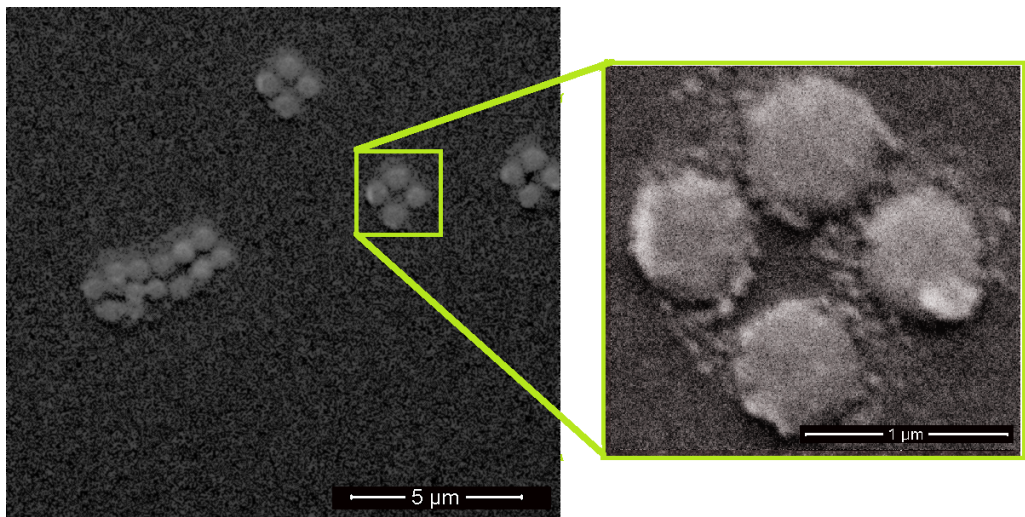
Figure 4.27: SEM pictures of 750 nm quadromer structures

4.4.3 Dimer Distance Variations

Several dimers are fabricated with different evaporation angles to comprehend nanometer scale distance control of HMCL. Thickness of the structures is 40 nm as in the previous set of samples. Higher amount of denting of holes for 262 nm samples resulted increased evaporation angle requirements for observation of nicely separated dimers. Moreover it is clear in figure 4.29(c) zoomed one, that uneven denting resulted varying inter-particle distances between individual particles. Inter particle distance of the dimer on the right side seems to be bigger because of less denting on that hole.
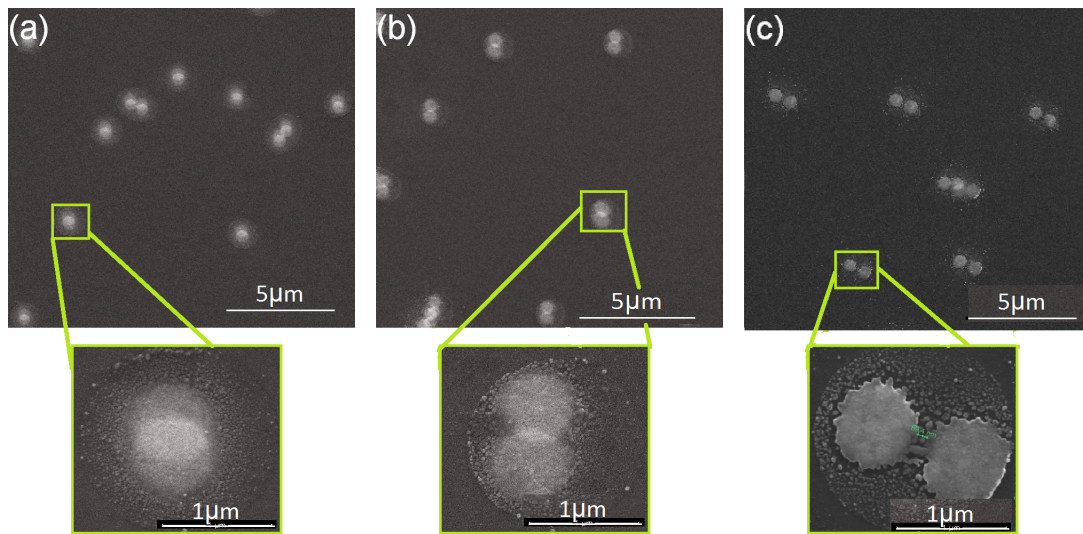
Figure 4.28: Dimer distance variations of dimers evaporated through 750 nm holes with (a) 13 degree (b) 18 degree (c) 22 degree evaporation angles.
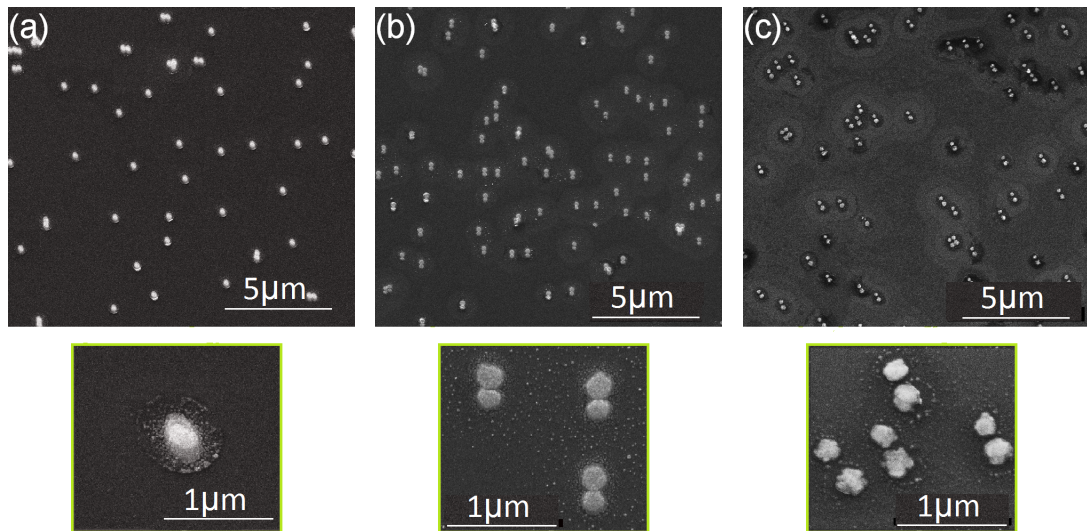
Figure 4.29: Dimer distance variations of dimers evaporated through 262 nm holes with (a) 15 degree (b) 20 degree (c) 25 degree evaporation angles.

4.5 Asymmetrical Geometries

To understand fabrication capabilities of asymmetrical structure geometries with HMCL; several experiments conducted. Three mechanisms are found that can be used to fabricate asymmetrical structures.

4.5.1 Asymmetrical Thickness Deposition

Asymmetrical structures can be generated by deposition of different thickness or different materials on different evaporation sessions. This process induces an asymmetry in z-axis. Z-axis asymmetry is highly unique to HMCL. Preliminary experiments on asymmetrical deposition are conducted with both 750 nm and 262 nm dimers. Both thickness asymmetries and material asymmetries fabricated. Dimers with respective thicknesses of; 40 nm to 60 nm, 40 nm to 75 nm, 80 nm to 120 nm and material asymmetries with 20 nm of Au to 40 nm of Ag deposited structures fabricated on large areas for both 750 nm and 262 nm holes. Optical reflection experiments are conducted to all the asymmetrical samples. However; no plasmonic resonance is detected. More through optical experiments should be conducted for decisive plasmonic characterization.

61
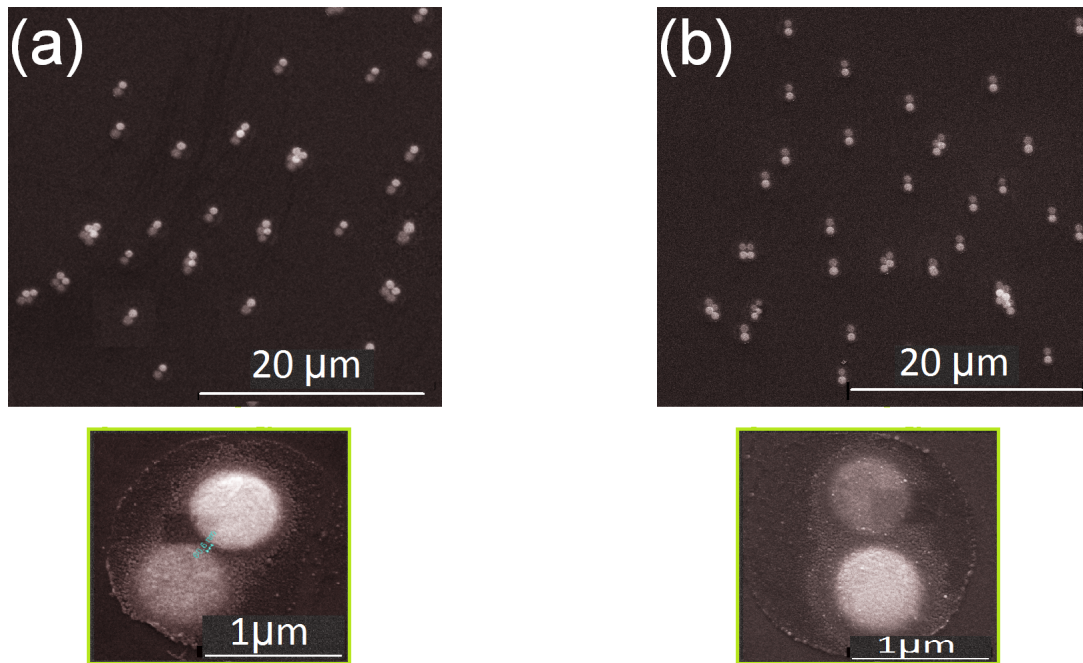
Figure 4.30: Asymmetrical dimers obtained by evaporation of Ag through 750nm holes (a) 40 nm to 60 nm (b) 40 nm to 75 nm asymmetry
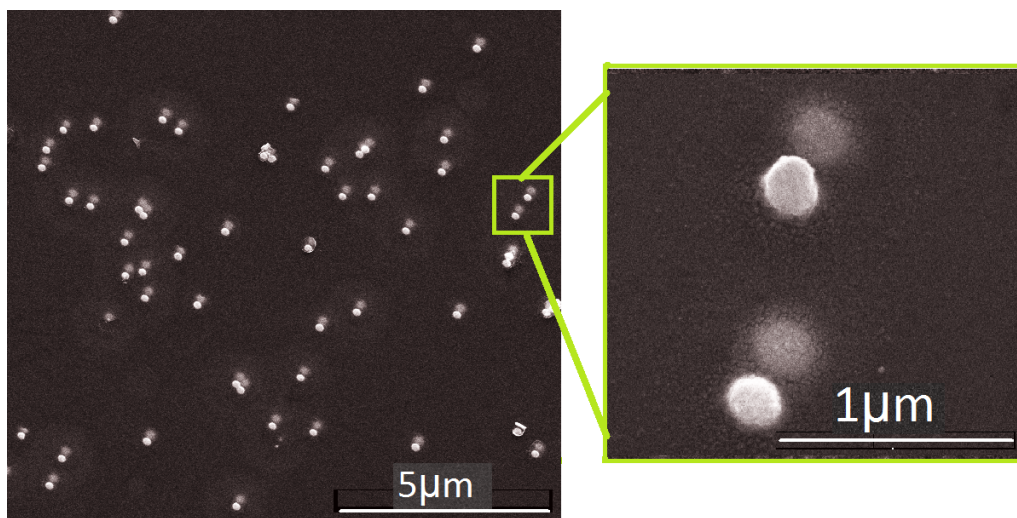
Figure 4.31: Ag - Au dimers with 40 nm to 20 nm thicknesses evaporated through 250 nm holes

4.5.2 Clogging Effect

Diameter of holes gets smaller as materials deposited through them, this effect is called clogging effect. Clogging effect limits fabricated structures to certain amount of total deposition thickness, that is bound to the hole diameter. Besides from the limitation this effect opens a new possibilities of geometries that can be generated by HMCL. As the hole diameter decreases the feature size of deposited material also decreases. Structures like pyramids or very small featured thin objects near a larger object can be fabricated. This effects bring a whole new level of symmetrical and asymmetrical structure possibilities. Clogging thickness to deposition thickness ratio is observed to be around 3/5 for 20 degrees angled deposition. Figure 4.32 shows, diameter of the holes after different amount of material deposition.
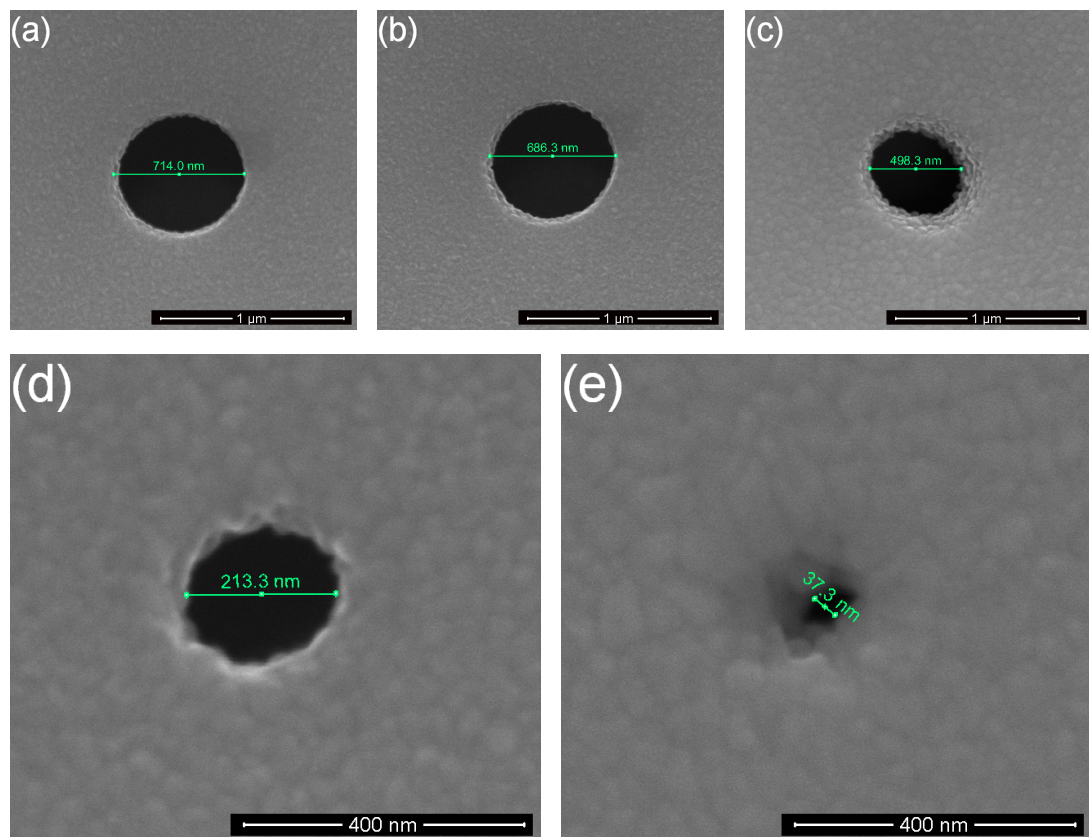
Figure 4.32: Clogging effect decreases the diameter of holes as material is deposited through them. (a)(b)(c) 60 nm, 120 nm and 400 nm material deposited respectively through initially 750 nm holes (d)(e) 120 nm and 400 nm material deposited respectively through 262 nm initial holes.

4.5.3 Asymmetrical Angle

Another Asymmetrical deposition possibility that stumbled upon through the experiments is, asymmetrical angled deposition. It is a little unconventional way of depositing asymmetries. If the width of generated undercuts are exactly known, desired portion of structure can be evaporated on the sidewalls on purpose. The portion evaporated on the sidewall removes with the removal of polymer film, leaving half disks on the surface. Structures in Figure 4.33 are asymmetrically evaporated with one session with 5 degrees azimuthal angle and other with 25 degrees azimuthal angle with 180 degree polar angle difference. As a result an interesting asymmetry is achieved.
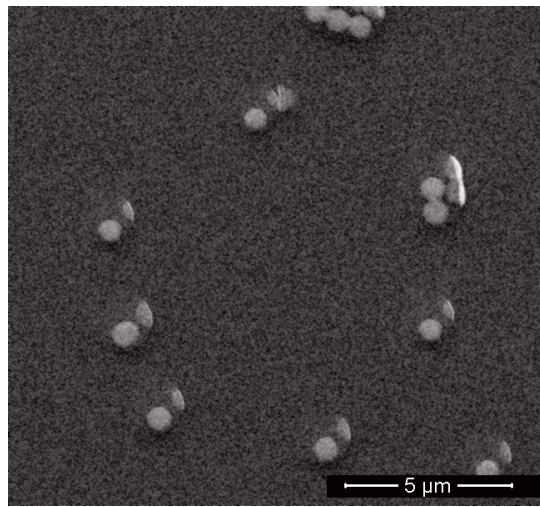
Figure 4.33: Asymmetrical structures fabricated by 5 degrees and 25 degrees asymmetrical evaporation angles through 750nm holes.

CHAPTER 5

CONCLUSIONS

5.1 Summary and Discussion

The work in this thesis is based on utilization of hole mask colloidal lithography and examination some of its fabrication capabilities. It has been shown that large area metal nanostructuring with highly controllable dimer distances and asymmetries can be fabricated with HMCL. Dimers, trimers and quadromers are successfully deposited, moreover controllable dimer distance variations achieved by altering the deposition angle. Several methods for fabricating asymmetries are found and asymmetrical structures fabricated with with different properties are fabricated on large areas. Utilization of HMCL consists of optimization of a procedure for obtaining appropriate hole mask with appropriate surface coverage of holes. Five main steps in the procedure can be identified as, sacrificial layer deposition, nanoparticle decoration, metal film coating, particle removal and undercutting the holes. Details of each process step and its importance is discovered, optimized and applied successfully for two different sizes of colloidal particles. Each of these step are examined with experiments and to comprehend effectiveness, optical microscope and scanning electron microscopy (SEM) characterizations are obtained. Examination of fabrication capabilities of HMCL conducted after procuring an optimized hole mask generation procedure. Positional precision and asymmetrical fabrication capabilities and possibilities have been examined and discussed.

One of the most important advantage of using photoresist as sacrificial layer and exposure and development to undercut would be possibility of generation larger undercut

widths at the surface compared to isotropic dry etching. Undercutting with exposure and developments has been investigated and partial success has been achieved. AZ 5214 image rehearsal photoresist is used as positive tone resist as it can give desired film thickness values. One of the drawbacks associated with the success of exposure and development undercutting is denting near the holes. This effect is probably caused by capillary forces while evaporation of water out of the surface. Denting effect can be compensated if all the dents are of equal depth, for 750 nm holes that was the case so denting effect is not really an important issue; however, different dent depths are observed when 262 nm holes are used. This difference greatly changes the position of deposition yielding structures with slightly different geometries. Strong control over deposition position is one of the most important property of HMCL and it is harmed by this effect with 262 nm particle sizes. The most probable explanation of uneven undercutting observed with 262 nm particles is malfunctioning photoresist and/or developer. The photoresist and its developer in use when the effect was observed was over 3 years passed its expiration date, there was some fresh one but it finished way before completion of procedure steps. Expired resists can grow discontinuities some solidification may take place on both resist and its developer causing small particles inside the solutions. these particles may block effective dissolution of exposed resist in the developer. These solids may be small enough that they does not effect (or slightly effects) dissolution through 750 nm holes while blocking effective dissolution through 262 nm holes. I think it is too soon to say that exposure and development undercutting is not successful for 262 nm holes since fresh chemicals can turn the tides.

Some of the other observations and findings that show up throughout the optimization experiments that worth mentioning can be listed as follows. It has been found that random electrostatic deposition well fits for the required application. Nanoparticle deposition surface coverage is found to be adjustable by both concentration of particle solution and adsorbed polyelectrolyte solution. Effective gold film deposition over the nanoparticles is another important issue of the process steps. As it is mentioned premature separation of particles is observed because of the force dynamics between adsorbed particles and charged surface of evaporated film, when the surface is not in electrical contact with the sample holder.

Examination of asymmetrical deposition possibilities yield that HMCL is very strong on fabrication of asymmetrical structures. Three mechanisms are observed that can be used for fabrication of asymmetric structures. Thickness asymmetry and size asymmetry employed by the clogging of holes can be considered as main asymmetrical applications. Deposition to sidewalls to obtain asymmetries is an unconventional way but still can be used to fabricate unconventional asymmetrical plasmonic nanoparticles.

One other issue to discuss about preliminary structures that the thermal evaporation seems to be not entirely directional. Some material is observed to be deposited on the different places on empty area under the holes (undercuts). The reason that we can observe the undercut width in figure 4.20 (b), is deposition of material into whole undercut area. This issue can be resulting from low vacuum pressure that is on the order of 10^{-5} torr. Increasing the evaporation speed can in some level overcome this problem since the evaporated material will travel faster thus probability of collusion will be lowered. A better vacuum system can also be used in future experiments.

Reflection measurements that conducted on generated dimer distance and asymmetry samples yield no (or undetectable) plasmonic signal. That may simply because of the resonance modes of silver particles of used dimensions falling outside of measurement spectral range. It is important to note that the thickness values of structures are solely chosen for imaging with SEM. A more comprehensive research will be made to determine fitting structure geometries that resonates at optical wavelengths in the near future for examination of optical properties.

5.2   A Glimpse to The Future

Although several experiments conducted and HMCL is successfully applied for preliminary structures, there are still much work to do until complete conquest of all properties that HMCL can support. One of the first things that will be produced is motorized evaporation holder. As it is mentioned in the beginning of chapter 4, a motorized evaporation holder can be used for fabricating very complex geometries. Actually, a coworker of mine Yusuf Kasap has been working on it for some time and
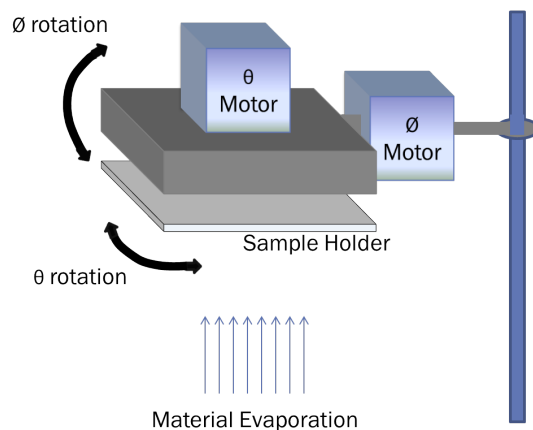
Figure 5.1: Angled deposition system that will be used in the near future

its in final states. This system will be employed in a very near future.

While experiments conducted with different particle sizes and freshly bought photoresist (already ordered), one of the periodic non-close packed deposition methods that are discussed at the end of chapter 3 will be optimized to generate periodic arrays. This will give us more control over surface coverage and a more uniform plasmonic response from the surface.

HMCL brings a new breath to surface nanostructuring technology. It is a novel method for fabricating large area nanostructures with complex, state of the art nano geometries. HMCL not only opens new doors for experimental examination of yet unexplored or partially explored areas in plasmonics; but also can match industrial throughput requirements such that proof of principle experiments can be industrialized immediately. Many previously conducted experiments can be reproduced without the area limitations of previously used methods and collective responses of complex geometries can be examined.

REFERENCES

[1] Richard P. Feynman. There's Plenty of Room at the Bottom. 1959.

[2] David a Schultz. Plasmon resonant particles for biological detection. *Curr. Opin. Biotechnol.*, 14(1):13–22, February 2003.

[3] Kadir Aslan, JR Lakowicz, and CD Geddes. Plasmon light scattering in biology and medicine: new sensing approaches, visions and perspectives. *Curr. Opin. Chem. Biol.*, 9(5):538–44, October 2005.

[4] Katherine a Willets and Richard P Van Duyne. Localized surface plasmon resonance spectroscopy and sensing. *Annu. Rev. Phys. Chem.*, 58:267–97, January 2007.

[5] ME Stewart and CR Anderton. Nanostructured plasmonic sensors. *ACS Chem. Rev.*, 108(2):494–521, March 2008.

[6] S. Nie. Probing Single Molecules and Single Nanoparticles by Surface-Enhanced Raman Scattering. *Science (80-.).*, 275(5303):1102–1106, February 1997.

[7] E C Le Ru, M Meyer, and P G Etchegoin. Proof of single-molecule sensitivity in surface enhanced Raman scattering (SERS) by means of a two-analyte technique. *J. Phys. Chem. B*, 110(4):1944–8, February 2006.

[8] Samuel L Kleinman, Emilie Ringe, Nicholas Valley, Kristin L Wustholz, Eric Phillips, Karl a Scheidt, George C Schatz, and Richard P Van Duyne. Single-molecule surface-enhanced Raman spectroscopy of crystal violet isotopologues: theory and experiment. *J. Am. Chem. Soc.*, 133(11):4115–22, March 2011.

[9] Hongwen Liu, Ling Zhang, Xingyou Lang, Yoshinori Yamaguchi, Hiroshi Iwasaki, Yasushi Inouye, Qikun Xue, and Mingwei Chen. Single molecule detection from a large-scale SERS-active Au Ag substrate. *Sci. Rep.*, 1:112, January 2011.

[10] Vivian E Ferry, Jeremy N Munday, and Harry a Atwater. Design considerations for plasmonic photovoltaics. *Adv. Mater.*, 22(43):4794–808, November 2010.

[11] Stephan Fahr, Carsten Rockstuhl, and Falk Lederer. Improving the efficiency of thin film tandem solar cells by plasmonic intermediate reflectors. *Photonics Nanostructures - Fundam. Appl.*, 8(4):291–296, September 2010.

[12] Wen Liu, Xiaodong Wang, Yueqiang Li, Zhaoxin Geng, Fuhua Yang, and Jinmin Li. Surface plasmon enhanced GaAs thin film solar cells. *Sol. Energy Mater. Sol. Cells*, 95(2):693–698, February 2011.

[13] T.L. Temple, G.D.K. Mahanama, H.S. Reehal, and D.M. Bagnall. Influence of localized surface plasmon excitation in silver nanoparticles on the performance of silicon solar cells. *Sol. Energy Mater. Sol. Cells*, 93(11):1978–1985, November 2009.

[14] Alpan Bek, Reiner Jansen, Moritz Ringler, Sergiy Mayilo, Thomas a Klar, and Jochen Feldmann. Fluorescence enhancement in hot spots of AFM-designed gold nanoparticle sandwiches. *Nano Lett.*, 8(2):485–90, February 2008.

[15] K Höflich, M Becker, G Leuchs, and S Christiansen. Plasmonic dimer antennas for surface enhanced Raman scattering. *Nanotechnology*, 185303, 2012.

[16] David P. Fromm, Arvind Sundaramurthy, P. James Schuck, Gordon Kino, and W. E. Moerner. Gap Dependent Optical Coupling of Single Bowtie Nanoantennas Resonant in the Visible. *Nano Lett.*, 4(5):957–961, May 2004.

[17] Wei Ding, Renaud Bachelot, Sergei Kostcheev, Pascal Royer, and Roch Espiau de Lamaestre. Surface plasmon resonances in silver Bowtie nanoantennas with varied bow angles. *J. Appl. Phys.*, 108(12):124314, 2010.

[18] Norbert Kroo, Sndor Varro, Gyozo Farkas, Peter Dombi, Daniel Oszetzky, Attila Nagy, and Aladar Czitrovszky. Nonlinear Plasmonics. *J. Mod. Opt.*, 55(19-20):3203–3210, November 2008.

[19] J. Butet, G. Bachelier, I. Russier-Antoine, F. Bertorelle, a. Mosset, N. Lascoux, C. Jonin, E. Benichou, and P.-F. Brevet. Nonlinear Fano profiles in the optical second-harmonic generation from silver nanoparticles. *Phys. Rev. B*, 86(7):075430, August 2012.

[20] Deniz Turkpence, Gursoy B Akguc, Alpan Bek, and Mehmet Emre Tasgin. Engineering nonlinear response of nanomaterials using Fano resonances. *J. Opt.*, 2:1–10, 2014.

[21] Jun Zhao, Bettina Frank, Frank Neubrech, Chunjie Zhang, Paul V Braun, and Harald Giessen. Hole-mask colloidal nanolithography combined with tilted-angle-rotation evaporation: A versatile method for fabrication of low-cost and large-area complex plasmonic nanostructures and metamaterials. *Beilstein J. Nanotechnol.*, 5:577–86, January 2014.

[22] H. Fredriksson, Y. Alaverdyan, A. Dmitriev, C. Langhammer, D. S. Sutherland, M. Zäch, and B. Kasemo. Hole Mask Colloidal Lithography. *Adv. Mater.*, 19(23):4297–4302, December 2007.

[23] Stefano Cataldo, Jun Zhao, Frank Neubrech, Bettina Frank, Chunjie Zhang, Paul V Braun, and Harald Giessen. Hole-mask colloidal nanolithography for large-area low-cost metamaterials and antenna-assisted surface-enhanced infrared absorption substrates. *ACS Nano*, 6(1):979–85, January 2012.

[24] Bettina Frank, Xinghui Yin, Martin Schäferling, Jun Zhao, Sven M Hein, Paul V Braun, and Harald Giessen. Large-area 3D chiral plasmonic structures. *ACS Nano*, 7(7):6321–9, July 2013.

[25] Michael Faraday. The Bakerian Lecture : Experimental Relations of Gold (and Other Metals) to Light. *Philos. Trans. R. Soc. London*, 147(1858):145–181, 1857.

[26] Richard Zsigmondy and Jerome Alexander. *Colloids and the ultramicroscope; a manual of colloid chemistry and ultramicroscopy*. New York, J. Wiley & Sons, 1909.

[27] G Mie. Beitrage zur Optik truber Medien, speziell kolloidaler Metallosungen. *Ann. Phys*, 1908.

[28] ML Brongersma and PG Kik. *Surface plasmon nanophotonics*. Springer, 2007.

[29] Chris D Geddes. *Reviews in Plasmonics 2010*, volume 2010 of *Reviews in Plasmonics*. Springer New York, New York, NY, 2012.

[30] R. W. Wood. On a Remarkable Case of Uneven Distribution of Light in a Diffraction Grating Spectrum. *Proc. Phys. Soc.*, 18:269–275, 1902.

[31] R. H. Ritchie, E. T. Arakawa, J. J. Cowan, and N. Hamm. Surface-Plasmon Resonance Effect in Grating Diffraction. *Phys. Rev. Lett.*, 21:1530–1533, 1968.

[32] D. Pines. Collective Energy Losses in Solids. *Rev. Mod. Phys.*, 28:184–198, 1956.

[33] T W Ebbesen, T Thio, H. J. Lezec, H. F. Ghaemi, and P. A. Wolff. Extraordinary optical transmission through subwavelength hole arrays. *Nature*, 391(6):1114–7, March 1998.

[34] L. Martín-Moreno, F. García-Vidal, H. Lezec, K. Pellerin, T. Thio, J. Pendry, and T. Ebbesen. Theory of Extraordinary Optical Transmission through Subwavelength Hole Arrays. *Phys. Rev. Lett.*, 86(6):1114–1117, February 2001.

[35] Stefan Alex Maier. *Plasmonics: Fundamentals and Applications*. Springer, 2007.

[36] Sergey V. Gaponenko. *introduction to Nanophotonics*. Cambridge University Press, 2010.

[37] A. Wokaun. Surface enhancement of optical fields. Mechanism and applications. *Mol. Phys.*, 56(1), 1985.

[38] Uwe Kreibig and Michael Vollmer. *Optical Properties of Metal Clusters*. Springer, 1995.

[39] R. W. Boyd. *Nonlinear optics*. Academic Press, 2008.

[40] Stefan a. Maier. *Plasmonics Fundamentals and Applications*. Springer, 2007.

[41] PB Johnson and RW Christy. Optical constants of the noble metals. *Phys. Rev. B*, 1318(1970), 1972.

[42] Mark I. Stockman. Nanoplasmonics: past, present, and glimpse into future. *Opt. Express*, 19(22):22029–22106, October 2011.

[43] Prashant K. Jain and Mostafa a. El-Sayed. Plasmonic coupling in noble metal nanostructures. *Chem. Phys. Lett.*, 487(4-6):153–164, March 2010.

[44] James J. Storhoff, Anne a. Lazarides, Robert C. Mucic, Chad a. Mirkin, Robert L. Letsinger, and George C. Schatz. What Controls the Optical Properties of DNA-Linked Gold Nanoparticle Assemblies? *J. Am. Chem. Soc.*, 122(19):4640–4650, May 2000.

[45] Prashant K. Jain, Wenyu Huang, and Mostafa a. El-Sayed. On the Universal Scaling Behavior of the Distance Decay of Plasmon Coupling in Metal Nanoparticle Pairs: A Plasmon Ruler Equation. *Nano Lett.*, 7(7):2080–2088, July 2007.

[46] Andrew L. Fussell, Antti Isomäki, and Clare J. Strachan. Nonlinear Optical Imaging Introduction and Pharmaceutical Applications. *Am. Pharm. Rev.*, 2013.

[47] Martti Kauranen and Anatoly V Zayats. Nonlinear plasmonics. *Nat. Photonics*, 6(October):737–748, 2012.

[48] AK Bates, M Rothschild, TM Bloomstein, T. H. Fedynyshyn, R. R. Kunz, V. Liberman, and M. Switkes. Review of technology for 157-nm lithography. *IBM J. Res. Dev.*, 45(5):605–614, 2001.

[49] Eric C. Spivey, Eric T. Ritschdorff, Jodi L. Connell, Christopher a. McLennon, Christine E. Schmidt, and Jason B. Shear. Multiphoton Lithography of Unconstrained Three-Dimensional Protein Microstructures. *Adv. Funct. Mater.*, 23(3):333–339, January 2013.

[50] Bryan Cord, Joel Yang, Huigao Duan, David C. Joy, Joseph Klingfus, and Karl K. Berggren. Limiting factors in sub 10 nm scanning electron beam lithography. *J. Vac. Sci. Technol. B Microelectron. Nanom. Struct.*, 27(6):2616, 2009.

[51] Huigao Duan, Donald Winston, Joel K. W. Yang, Bryan M. Cord, Vitor R. Manfrinato, and Karl K. Berggren. Sub-10-nm half-pitch electron-beam lithography by using poly(methyl methacrylate) as a negative resist. *J. Vac. Sci. Technol. B Microelectron. Nanom. Struct.*, 28(6):C6C58, 2010.

[52] Vitor R Manfrinato, Lihua Zhang, Dong Su, Huigao Duan, Richard G Hobbs, Eric a Stach, and Karl K Berggren. Resolution limits of electron-beam lithography toward the atomic scale. *Nano Lett.*, 13(4):1555–8, April 2013.

[53] http://www.phy.cam.ac.uk/research/research-groups/sp/facilities/ebl. *Cambridge Univ. Dep. Physics. Last access, August 2014.*

[54] Ampere a. Tseng, Andrea Notargiacomo, and T. P. Chen. Nanofabrication by scanning probe microscope lithography: A review. *J. Vac. Sci. Technol. B Microelectron. Nanom. Struct.*, 23(3):877, 2005.

[55] R. D. Piner. "Dip-Pen" Nanolithography. *Science (80-.).*, 283(5402):661–663, January 1999.

[56] Alongkorn Pimpin and Werayut Srituravanich. Review on Micro- and Nanolithography Techniques and their Applications. *Eng. J.*, 16(1):37–56, January 2012.

[57] MF Crommie, CP Lutz, and DM Eigler. Confinement of electrons to quantum corrals on a metal surface. *Science (80-.).*, 1993.

[58] Uwe Stamm. Extreme ultraviolet light sources for use in semiconductor lithography: state of the art and future development. *Appl. Phys.*, 37(23):3244–3253, December 2004.

[59] Banqiu Wu and Ajay Kumar. Extreme ultraviolet lithography: A review. *J. Vac. Sci. Technol. B Microelectron. Nanom. Struct.*, 25(6):1743, 2007.

[60] Rajesh Menon, Amil Patel, Dario Gil, and Henry I. Smith. Maskless lithography. *Mater. Today*, (February):26–33, 2005.

[61] Seung-Man Yang, Se Gyu Jang, Dae-Geun Choi, Sarah Kim, and Hyung Kyun Yu. Nanomachining by colloidal lithography. *Small*, 2(4):458–75, April 2006.

[62] Junhu Zhang, Yunfeng Li, Xuemin Zhang, and Bai Yang. Colloidal self-assembly meets nanofabrication: from two-dimensional colloidal crystals to nanostructure arrays. *Adv. Mater.*, 22(38):4249–69, October 2010.

[63] Nicolas Vogel. *Surface patterning with colloidal monolayers*. Springer Theses, 2012.

[64] H. J Butt, K. Graf, and M. Kappl. *Physics and chemistry of interfaces*. Weinheim: Wiley, 2006.

[65] P Somasundaran. *Deposition of latex particles: Theoretical and Experimental aspects*. Allied Publishers, 1995.

[66] Yue Li, Eun Lee, Weiping Cai, Ki Yup Kim, and Sung Oh Cho. Unconventional Method for Morphology Controlled Carbonaceous Nanoarrays Polystyrene Colloidal Monolayer. *Am. Chem. Soc.*, 2(6):2–6, 2008.

[67] Alfred Plettl, Fabian Enderle, Marc Saitner, Achim Manzke, Christian Pfahler, Stefan Wiedemann, and Paul Ziemann. Non-Close-Packed Crystals from Self-Assembled Polystyrene Spheres by Isotropic Plasma Etching: Adding Flexibility to Colloid Lithography. *Adv. Funct. Mater.*, 19(20):3279–3284, October 2009.

[68] Jae Joon Kim, Yue Li, Eun Je Lee, and Sung Oh Cho. Fabrication of size-controllable hexagonal non-close-packed colloidal crystals and binary colloidal crystals by pyrolysis combined with plasma-electron coirradiation of polystyrene colloidal monolayer. *Langmuir*, 27(6):2334–9, March 2011.

[69] Xin Yan, Jimin Yao, Guang Lu, Xiao Li, Junhu Zhang, Kun Han, and Bai Yang. Fabrication of non-close-packed arrays of colloidal spheres by soft lithography. *J. Am. Chem. Soc.*, 127(21):7688–9, July 2005.

[70] Xiao Li, Tieqiang Wang, Junhu Zhang, Xin Yan, Xuemin Zhang, Difu Zhu, Wei Li, Xun Zhang, and Bai Yang. Modulating two-dimensional non-close-packed colloidal crystal arrays by deformable soft lithography. *Langmuir*, 26(4):2930–6, March 2010.

[71] Srinivasan Venkatesh, Peng Jiang, and Bin Jiang. Generalized fabrication of two-dimensional non-close-packed colloidal crystals. *Langmuir*, 23(15):8231–5, July 2007.

[72] Lucio Isa, Karthik Kumar, Mischa Müller, Jan Grolig, Marcus Textor, and Erik Reimhult. Particle lithography from colloidal self-assembly at liquid-liquid interfaces. *ACS Nano*, 4(10):5665–70, October 2010.

[73] Nicolas Vogel, Sebastian Goerres, Katharina Landfester, and Clemens K. Weiss. A Convenient Method to Produce Close- and Non-close-Packed Monolayers using Direct Assembly at the Air-Water Interface and Subsequent Plasma-Induced Size Reduction. *Macromol. Chem. Phys.*, 212(16):1719–1734, August 2011.

[74] Martin R. Widmer, Manfred Heuberger, Janos Vörös, and Nicholas D. Spencer. Influence of polymer surface chemistry on frictional properties under protein-lubrication conditions: implications for hip-implant design. *Tribol. Lett.*, 10:111–116, 2001.

[75] M.T. Khorasani and H. Mirzadeh. Effect of oxygen plasma treatment on surface charge and wettability of PVC blood bag. *Radiat. Phys. Chem.*, 76(6):1011–1016, June 2007.

74

[76] Mark C Barnes, Doh-Y Kim, Hyo S Ahn, Chang O Lee, and Nong M Hwang. Deposition mechanism of gold by thermal evaporation: approach by charged cluster model. *J. Cryst. Growth*, 213(1-2):83–92, May 2000.